

Supporting Information

High-performance aqueous sodium-ion/sulfur battery using elemental sulfur

Mukesh Kumar, Neha Thakur, Ankur Bordoloi, Ashok Yadav, Shambhunath Jha, Dibyendu Bhattacharyya, Debaprasad Mandal and Tharamani C. Nagaiah*

Experimental Details

Materials and reagents:

The following chemicals were used as received without any further purification. Nickel chloride extra pure (hexahydrate) (97%, crystalline), ammonium metavanadate (99%, crystalline), ammonium fluoride (98%, crystalline), and red phosphorus (98%, crystalline) were procured from Loba Chemie. Sodium sulfate and sublimed sulfur powder were from Alfa-Aesar. Urea, isopropyl alcohol, Triton X-100, H₂O₂ (30 %) were procured from Merck. Nafion N-117 membrane was purchased from the Fuel Cell Stores. Deionized water was obtained from a Millipore system (>12 MΩ cm⁻¹).

Physical characterization: As prepared, anode catalysts before and after S incorporation were characterized using X-ray powder diffraction (XRD), and the diffraction patterns were recorded using PANalytical X'PERT pro diffractometer in the 2θ range of 5-80° with a scan speed of 2° per minute using CuKα radiation (λ=0.1542 nm, 40kV, 40mA) and a proportional counter detector. The morphology of all the anode materials were evaluated by scanning electron microscopy (SEM) using JEOL JSM-6610LV. The elemental distribution was analyzed using energy dispersive X-ray analysis (EDX; Oxford, INCAx-act, 51-ADD0013). In-depth morphology and elemental distribution by Transmission electron microscopy (TEM) and high-resolution TEM (HR-TEM) images were recorded using a JEM 2100 (JEOL, Japan) operating at 200 keV. The oxidation state of the elements before and after the charge-discharge analysis was evaluated by X-ray photoelectron spectroscopy (XPS) using Thermo scientific NEXSA surface analysis with a micro-focused (400 μm, 72 W, 12000 V) monochromatic Al Kα (1486.6 eV) a hemispherical analyzer and under ultrahigh vacuum (UHV 8-10 mbar). The obtained spectra were calibrated with C 1s

spectra. UV-Vis measurements were performed using the Shimadzu UV-2600 spectrophotometer. The XAS measurements were carried out at the Energy-Scanning EXAFS beamline (BL-9) at the Indus-2 Synchrotron Source (2.5 GeV, 100 mA). This beamline operates in the energy range of 4 KeV to 25 KeV. The beamline optics consists of a Rh/Pt coated collimating meridional cylindrical mirror and the collimated beam reflected by the mirror is monochromatized by a Si(111) ($2d = 6.2709 \text{ \AA}$) based double crystal monochromator (DCM). The second crystal of DCM is a sagittal cylinder used for horizontal focusing, while a Rh/Pt coated bendable post mirror facing down was used for vertical focusing of the beam at the sample position. Rejection of the higher harmonics content in the X-ray beam was performed by detuning the second crystal of DCM. In the present case, XAS measurements were performed in transmission mode at Ni K-edge and V K-edge.

Na₂S adsorption study:

To verify the anchoring ability of various catalysts towards the discharge product, an adsorption study was performed for NiVP/Pi, NiVP/Pi-NCS, and NCS by considering Na₂S as a symbolic discharge product in the electrolyte (due to the high solubility of Na₂S in water because of its more polar nature). 10 mg of various catalysts were added to 3 mL of 3 mM Na₂S solution and sonicated for 10 minutes. Afterward, the solution was allowed to stand for 30 minutes while simultaneously capturing the optical images of change in electrolyte color.

Thermogravimetric analysis (TGA):

The thermogravimetric analysis (TGA) was performed in the N₂ atmosphere using alumina pan using “TGA/DSC1” instrument from Mettler Toledo with SDTA sensor, and data were analyzed in STAR^e software (version 12.1). Thermal stability was investigated by heating from 30 °C to 800 °C at a heating rate of 10 °C/min at 40 mL/min N₂ (99.999%) flow. Each sample was tested at least three times, and the error limit is <2%.

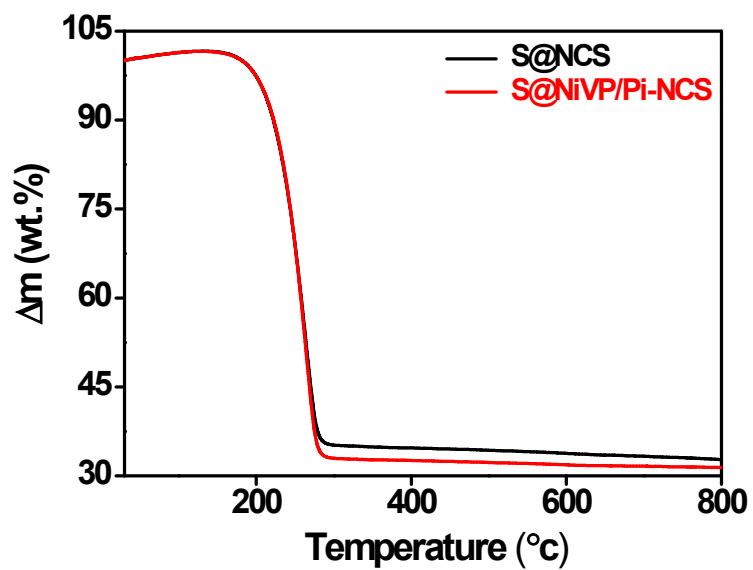


Fig. S1. TGA of S@NCS and S@NiVP/Pi-NCS.

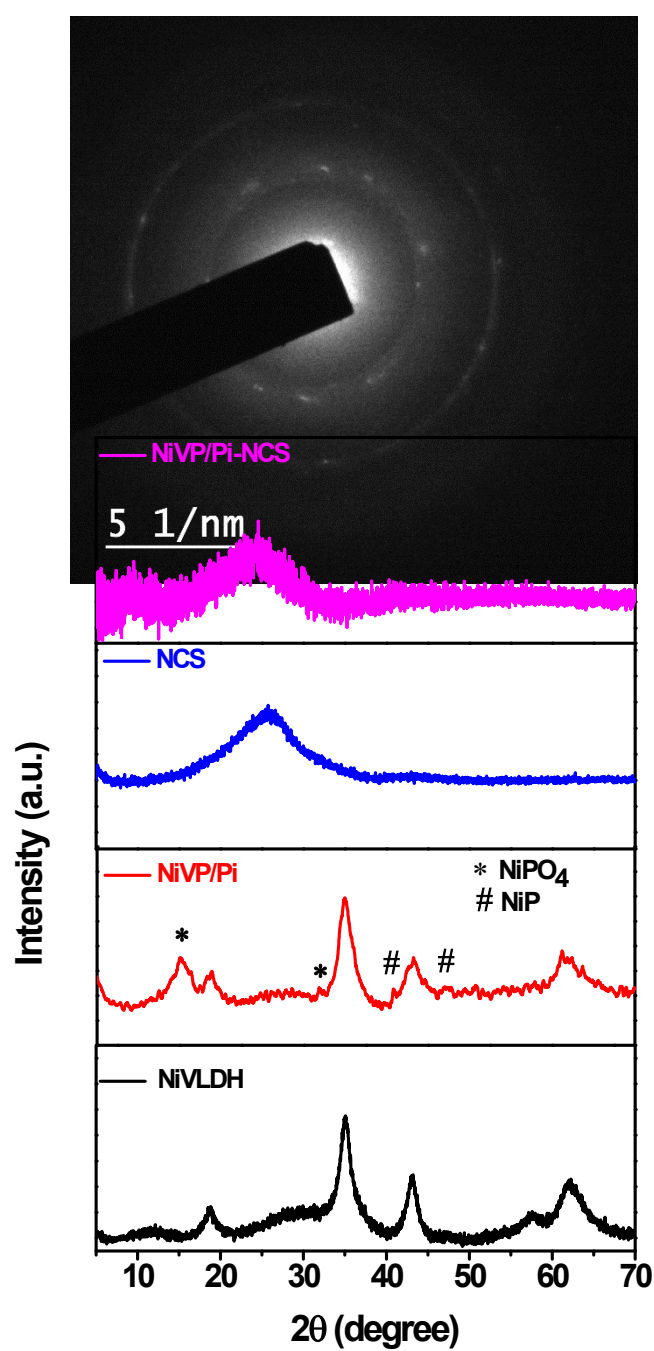


Fig. S2. SAED pattern

of NiVP/Pi catalyst.

Fig. S3. PXRD spectra of the various catalysts.

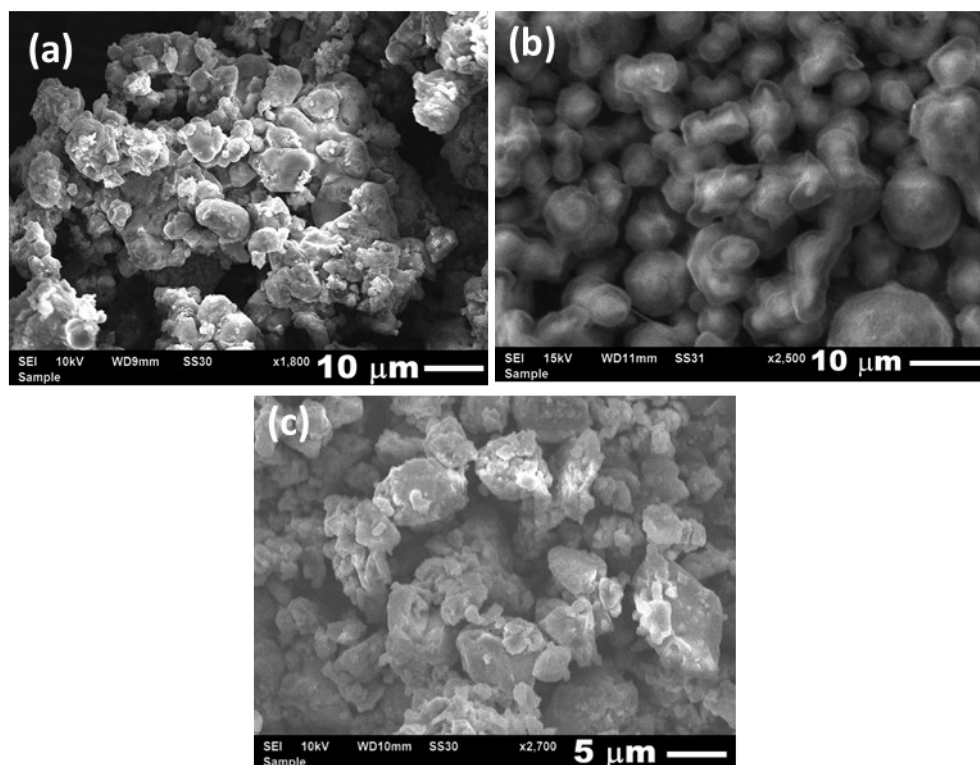


Fig. S4. SEM images of (a) NiVP/Pi-NCS, (b) S@NCS, (c) S@NiVP/Pi-NCS.

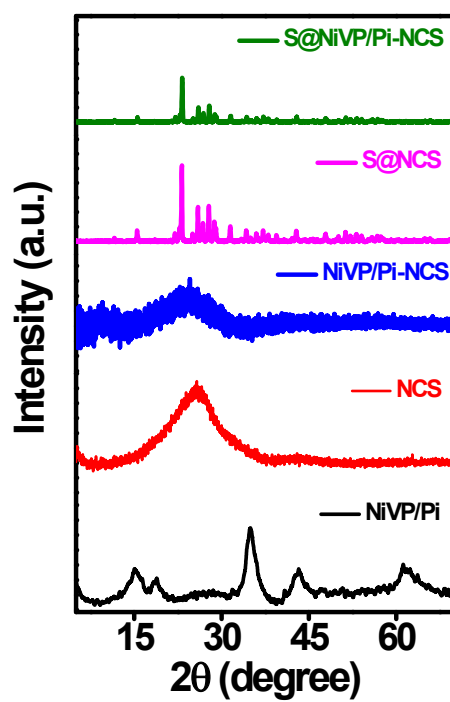


Fig. S5. PXRD spectra of various anode catalyst before and after the S incorporation.

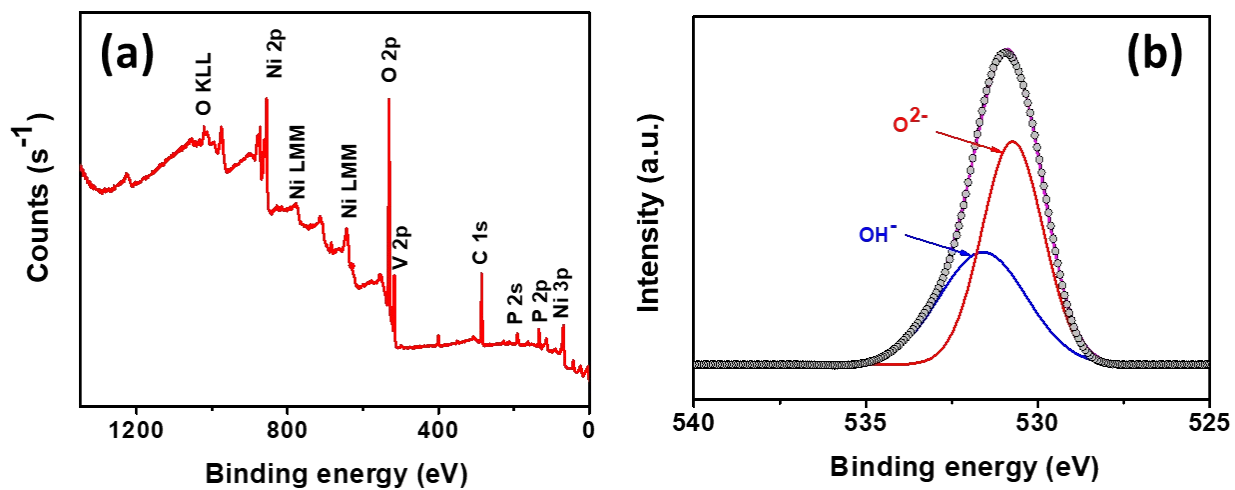


Fig. S6. (a) XPS survey spectrum and deconvoluted XP spectra (b) of O 1s for NiVP/Pi catalyst.

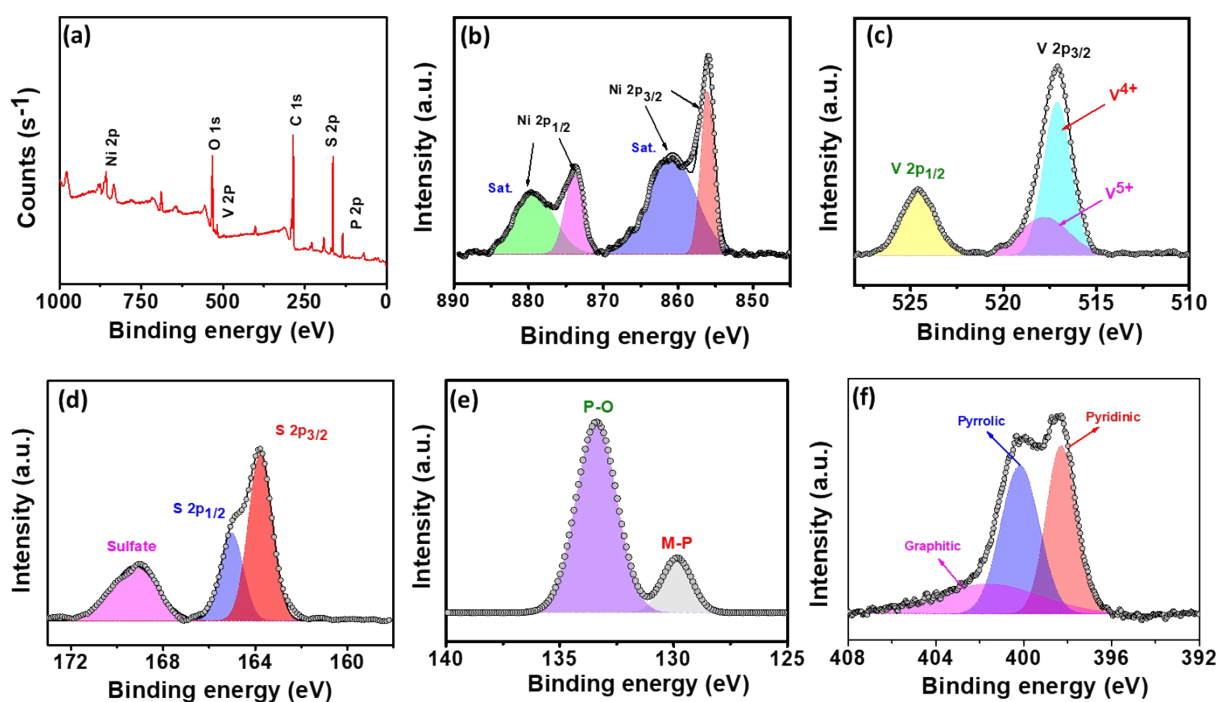
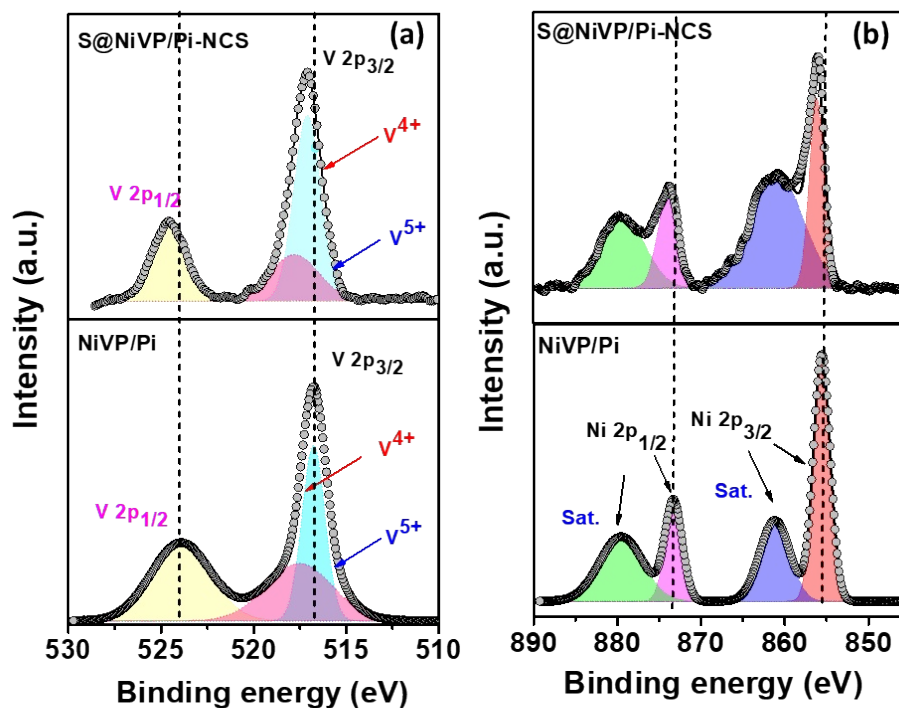


Fig. S7. (a) XPS survey spectra, (b) Ni 2p, (c) V 2p, (d) S 2p, (e) P 2p, and (f) N 1s of NCS anode.



XPS survey deconvoluted (b) Ni 2p, (c) V 2p, (d) S 2p, (e) P 2p, and (f) N 1s of S@NiVP/Pi-NCS anode.

Fig. S8. Comparison of deconvoluted XP spectra of (a) V 2p and (b) Ni 2p of S@NiVP/Pi-NCS and NiVP/Pi.

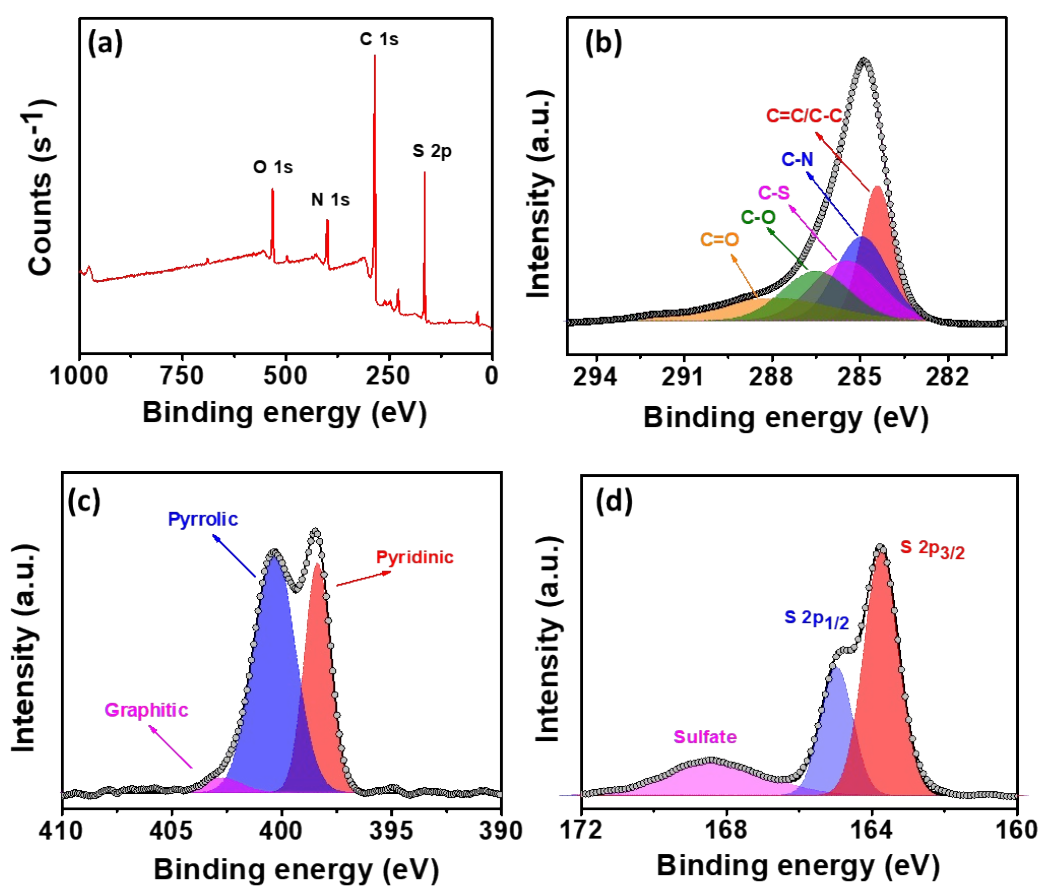


Fig. S9. (a) XPS survey spectra and deconvoluted XP spectra for (b) C 1s, (c) N 1s, and (d) S 2p, of S@NCS.

For S@NCS, the C 1s XP spectra in Fig. S9b deconvoluted into five peaks. Two major peaks at 284.5 and 285.0 eV correspond to sp^2 graphitic-like and sp^3 diamond-like carbon overlapped with sp^2 carbon bonded with nitrogen, beside peaks at 286.1 and 288.7 eV are assigned to the surface oxygen group. And another peak at 285.3 eV was assigned to the C-S bond. The N 1s spectra in Fig. S9c can be deconvoluted into three peaks at 398.4, 399.3, and 402.8 eV, corresponds to the presence of pyridinic, pyrrolic, and graphitic nitrogen. The S 2p spectra in Fig. S9d revealed three fitted peaks of sulfur, a pair of peaks at 163.8 and 164.98 eV are due to S $2p_{3/2}$ and S $2p_{1/2}$ of elemental S, and another peak located at 169.0 eV arise due to sulfate formation.

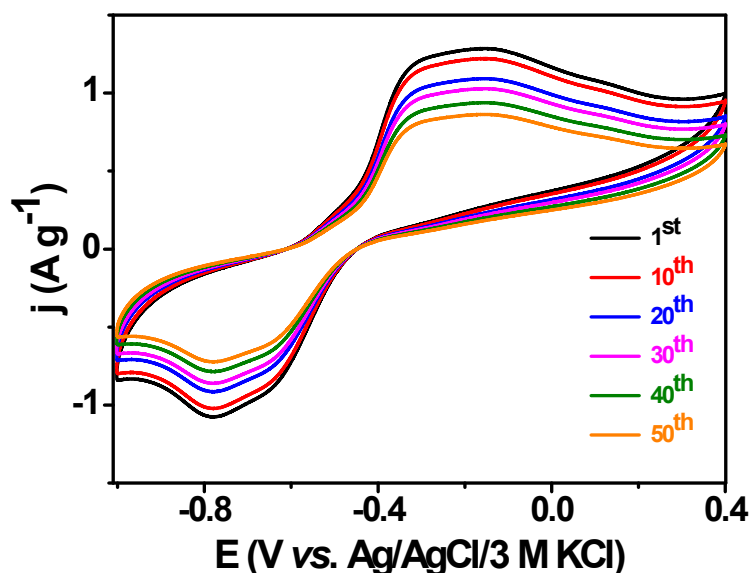


Fig. S10. Cyclic voltammograms of S@NCS at 2 mV s^{-1} after various cycles in 2 M aq. Na_2SO_4 electrolyte, CE: stainless steel (SS 316), RE: Ag/AgCl/3 M KCl.

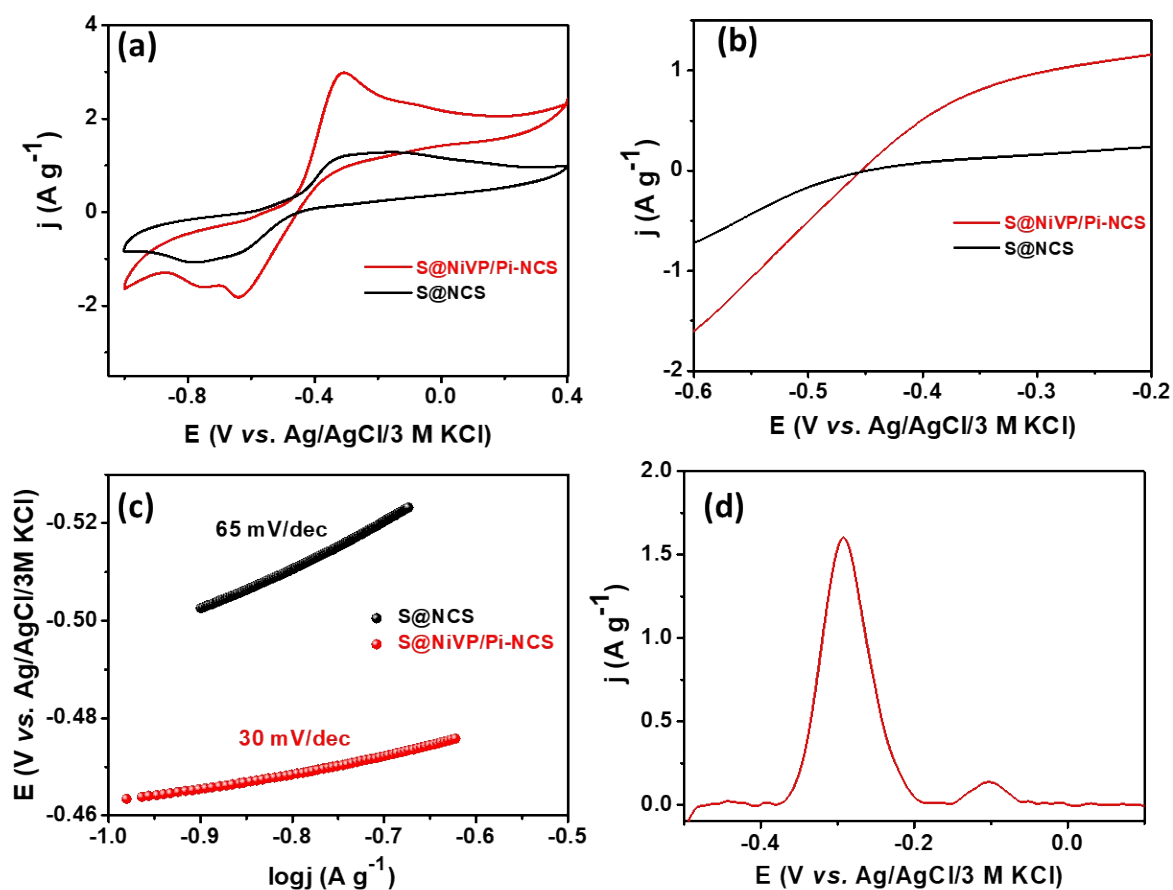


Fig. S11A. (a) Comparative cyclic voltammograms of S@NiVP/Pi-NCS and S@NCS anode in 2 M aq. Na₂SO₄ electrolyte at a scan rate of 2 mV s⁻¹, CE: stainless steel (SS 316), RE: Ag/AgCl/3 M KCl, (b) zoomed part of the CV and (c) corresponding Tafel plot for reduction (d) DPV of S@NiVP/Pi-NCS.

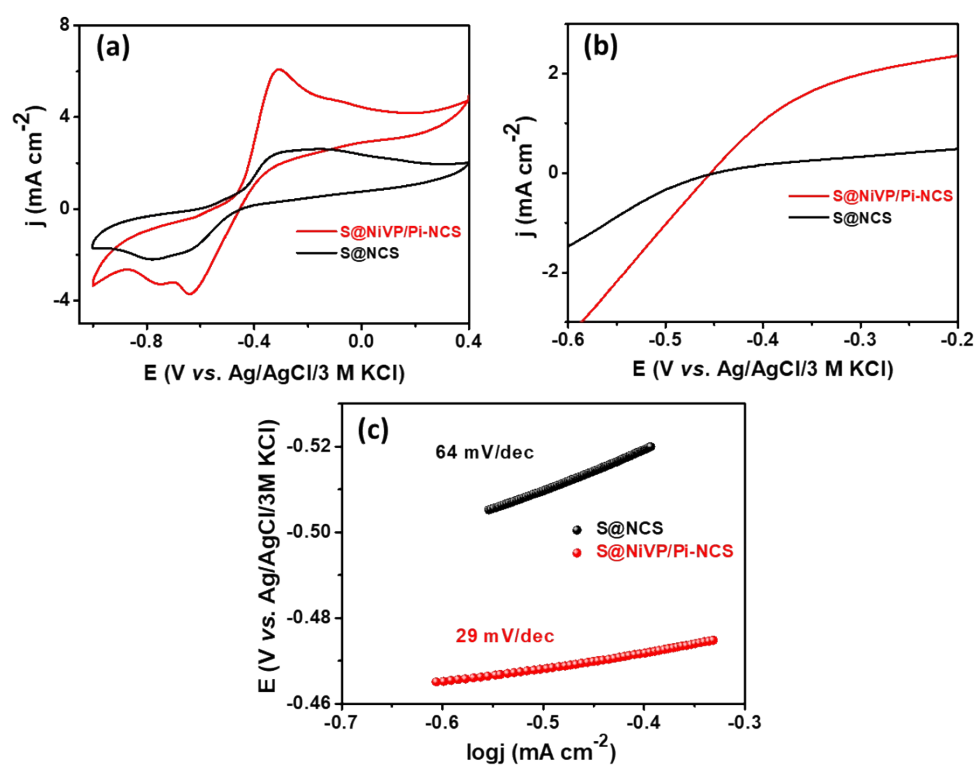


Fig. S11B. (a) Comparative cyclic voltammograms of S@NiVP/Pi-NCS and S@NCS anode in 2 M aq. Na₂SO₄ electrolyte at a scan rate of 2 mV s⁻¹, CE: stainless steel (SS 316), RE: Ag/AgCl/3 M KCl, (b) zoomed part of the CV and (c) corresponding Tafel plot for reduction

The diffusion constant is calculated by using calculated Randles–Sevcik

$$i_p = 0.4463 nFAC \left(\frac{nFvD}{RT} \right)^{\frac{1}{2}} \text{ equation}^1$$

-----(3)

Where I_p is the peak current in ampere, n is the number of electrons transfer in the reaction, A is the geometrical area of the electrode, C is the concentration of Na⁺, v represents the scan rate, D is the diffusion coefficient for Na⁺ ion, R is the gas constant, and T is the temperature.

To strengthened the point of kinetic enhancement, activation energy (E_a) was further evaluated from the Arrhenius equation for both the reduction (sodiation) and oxidation (desodiation) by performing CV at different temperatures from 10 °C-50 °C. As expected, peak current increases with an increase in temperature due to the increasing rate of reaction (Figs. S12a & S12b). From the slope of Arrhenius plot Fig. S12c and S12d, E_a was calculated for Na⁺ diffusion and polysulfide formation and was found to be 1.1 times lower for both oxidation and reduction of polysulfide for S@NiVP/Pi-NCS (Table S1), signifying the tendency of the catalyst to lower the activation barrier for Na-ion diffusion during S₈ to polysulfide formation and *vice versa*.

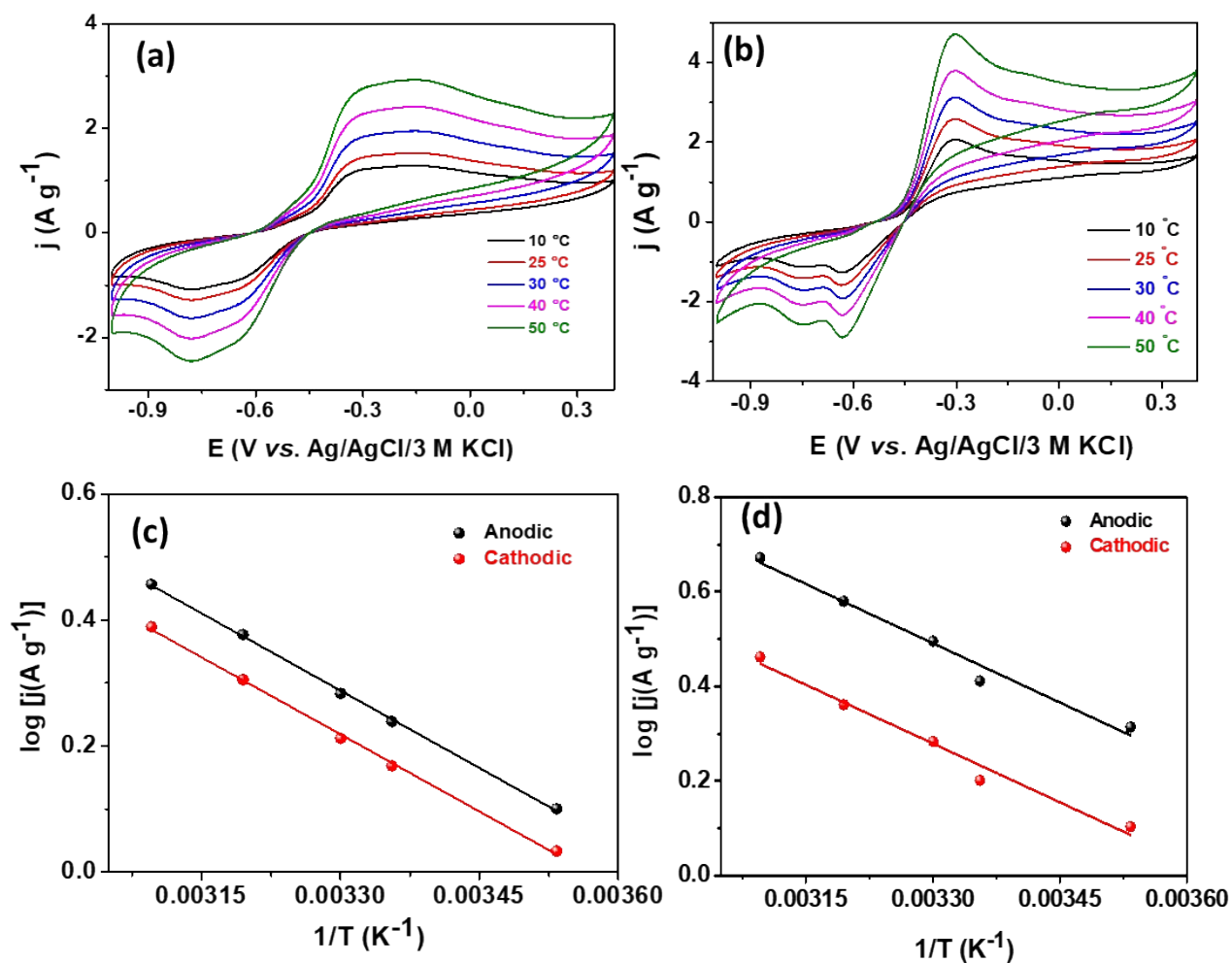


Fig. S12. Cyclic voltammograms of (a) S@NCS and (b) S@NiVP/Pi-NCS anode at various temperature in 2 M aq. Na₂SO₄ electrolyte at a scan rate of 2 mV s⁻¹ (c) and (d) are corresponding Arrhenius plots, CE: stainless steel (SS 316), RE: Ag/AgCl/3 M KCl.

Table S1: Comparison of activation energy calculated from the Arrhenius plot for both anodic and cathodic peak

Anode	slope		Ea (Kj mol ⁻¹)	
	Anodic	cathodic	Anodic	cathodic
S@NCS	893	815	17.1	15.64
S@NiVP/Pi-NCS	835	550	16	10.5

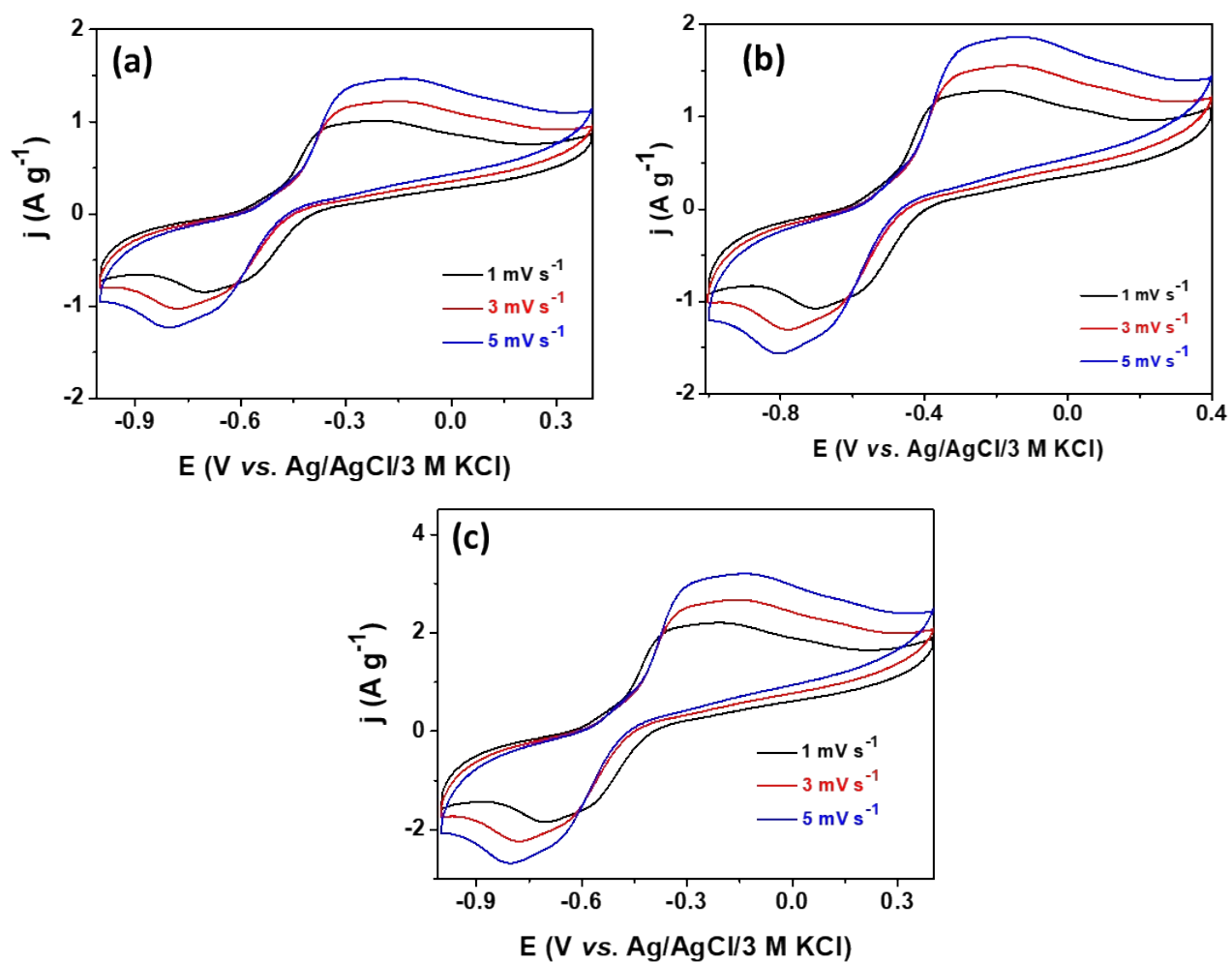


Fig. S13. Cyclic voltammograms of S@NCS anode at (a) 10 °C (b) 25 °C and (c) 40 °C respectively at various scan rates in 2 M aq. Na₂SO₄ electrolyte, CE: stainless steel (SS 316), RE: Ag/AgCl/3 M KCl.

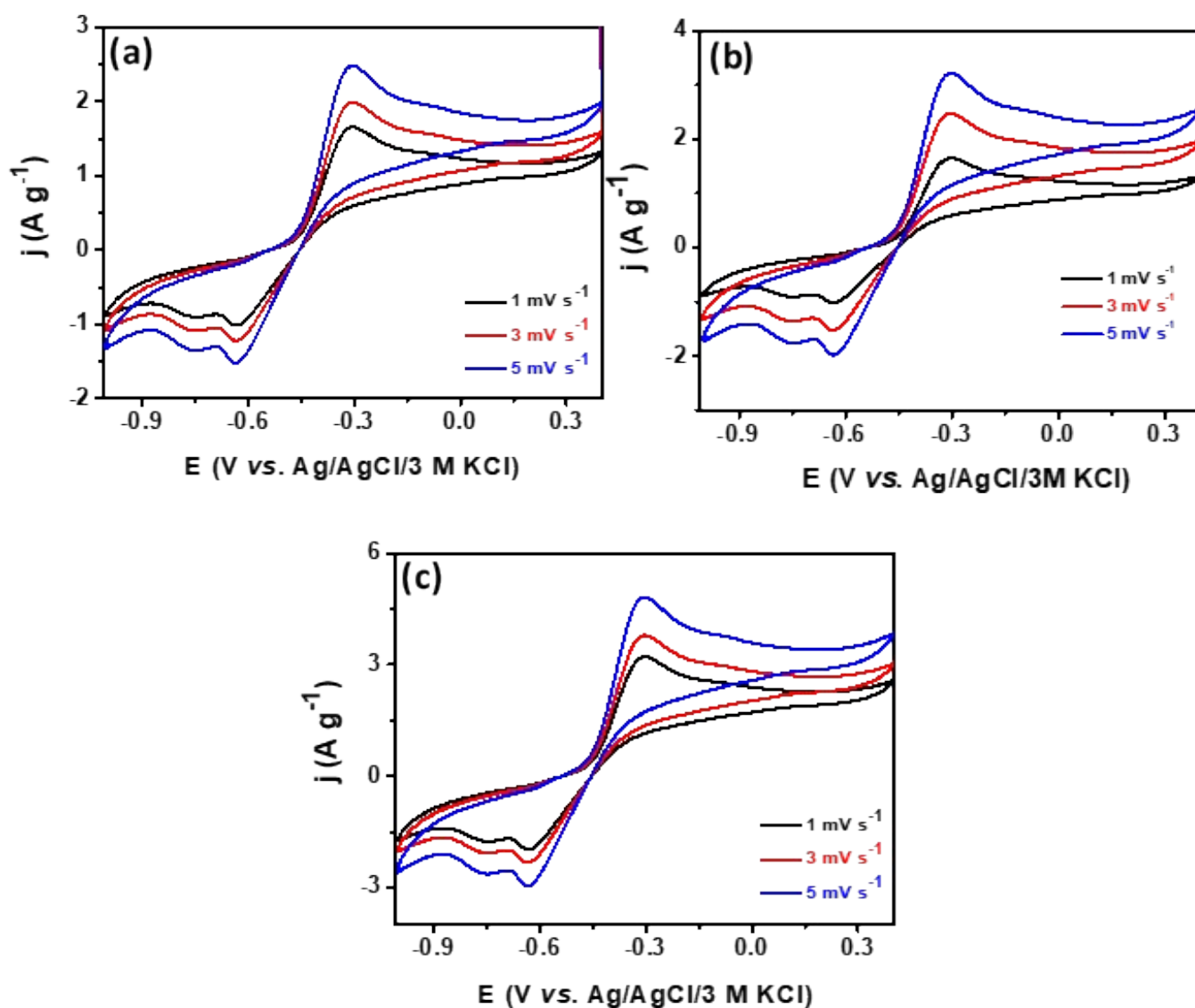


Fig. S14. Cyclic voltammograms of S@NiVP/Pi-NCS anode at (a) 10 °C (b) 25 °C and (c) 40 °C respectively at various scan rates in 2 M aq. Na_2SO_4 electrolyte, CE: stainless steel (SS 316), RE: Ag/AgCl/3 M KCl.

Calculation of Activation energy:

To calculate the activation energy and correlate it with the diffusion of Na^+ , initially, CV tests were performed under different scan rates (1, 3, and 5 mV s^{-1}) at three different temperatures (0 °C, 25 °C, 40 °C) as shown Fig. S13 and S14. The detailed procedure to calculate the activation energy of sodiation of S during discharge and desodiation of polysulfide during charge is detailed below. The plot of cathodic and anodic peak current densities of S@NCS and S@NiVP/Pi-NCS against the square root of the scan rates at various temperatures was found to be linear, indicating the process under diffusion control. The slopes (h)

of the above plot positively correlated to the corresponding Na^+ diffusion coefficient according to the classical Randles Sevcik equation.¹

$$i = 0.4463 nFA C(nFvD/RT)^{1/2} \text{-----}(1)$$

where i is the peak current,

n is the number of electrons per reaction species,

F is Faraday's constant (96485 C/mol),

A is the active electrode area,

R is the universal gas constant (8.314 J/mol K),

C is the Na^+ concentration, v is the scan rate,

D is the Na^+ diffusion coefficient,

T is the absolute temperature (K).

This equation can be more precisely written in the form of:

$$i = (4.64 \times 106) n^{1.5} A D^{0.5} C v^{0.5} T^{-0.5} \text{-----} (2)$$

n , A , and C are constants in a particular reaction, and the relationship could be simplified, and slope of current against the square root of scan rate can be written in the form of equation 3, which clearly indicate that Na^+ diffusion coefficient (D) is directly proportional to the square of the slope (h) and the absolute temperature T .

$$h = r D^{0.5} T^{-0.5} \text{----}(3)$$

$$h^2 T = r^2 D \text{-----}(4)$$

where r^2 is considered to be a constant for one particular system. We can write the diffusion related to activation energy in this form:

$$D = D_0 e^{-E_a/kT} \text{-----}(5)$$

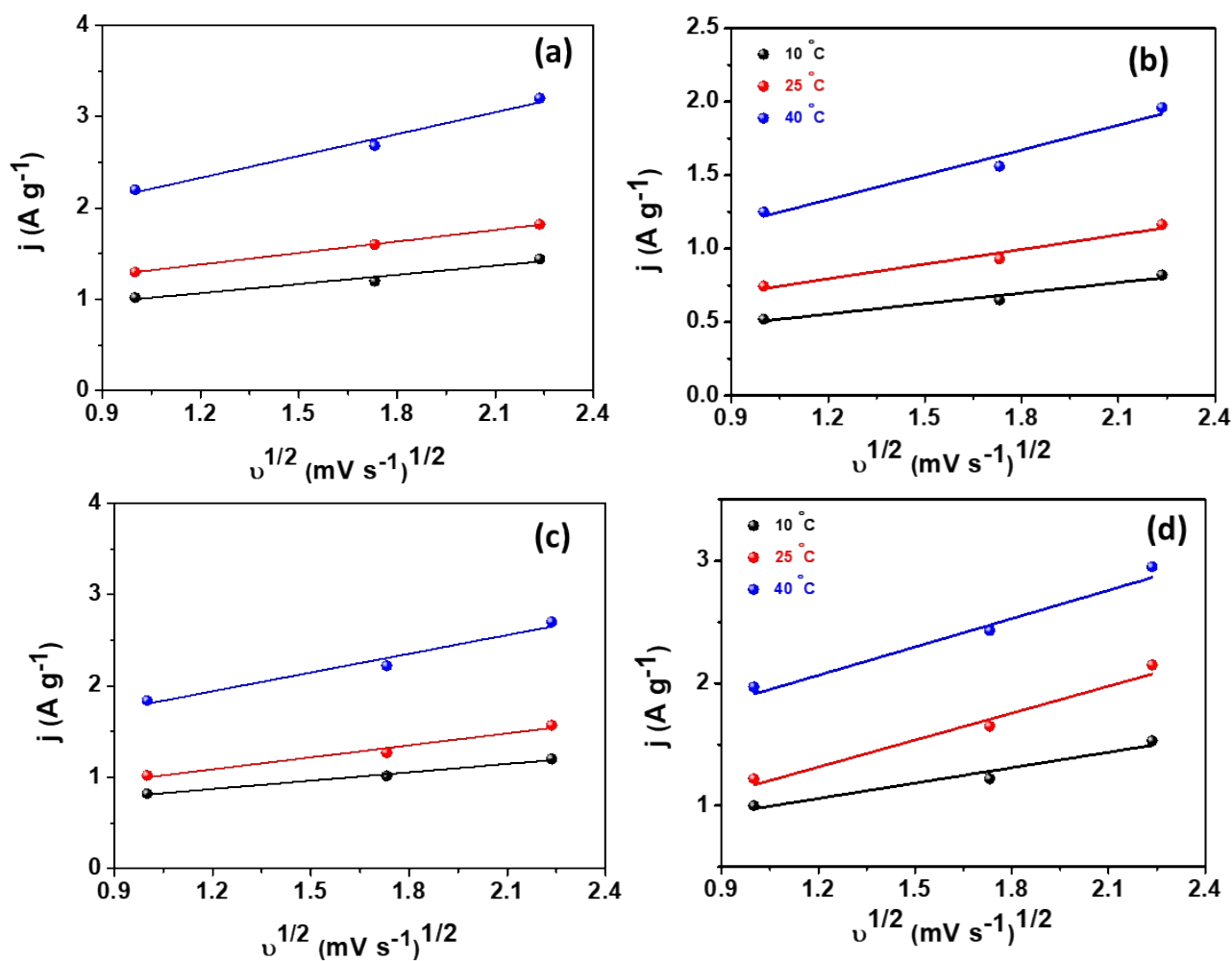
D_0 is the pre-exponential factor. E_a is the activation energy, k is the Boltzmann's constant. This equation can be more simplified by taking the logarithm of both side

$$\log D = -E_a/kT + \log D_0 \text{-----}(6)$$

by combining (4) and (6),

$$\log h^2T = -Ea/kT + \log D_0 \text{ -----(7)}$$

From equation (7) it is clear that the activation energy is equal to the slope of $\log h^2T$ against $1/T$.² The plot follows a linear relation in the temperature range of 10 – 40 °C. For the quantitative comparison, the value of activation energy was calculated for both anodic and cathodic peak current for both anodes and



summarised in Table S2.

Fig. S15. Plot of (a and c) anodic and (b and d) cathodic current density against the square root of scan rates for S@NCS and S@NiVP/Pi-NCS anode respectively in 2 M aq. Na₂SO₄ electrolyte, CE: stainless steel (SS 316), RE: Ag/AgCl/3 M KCl.

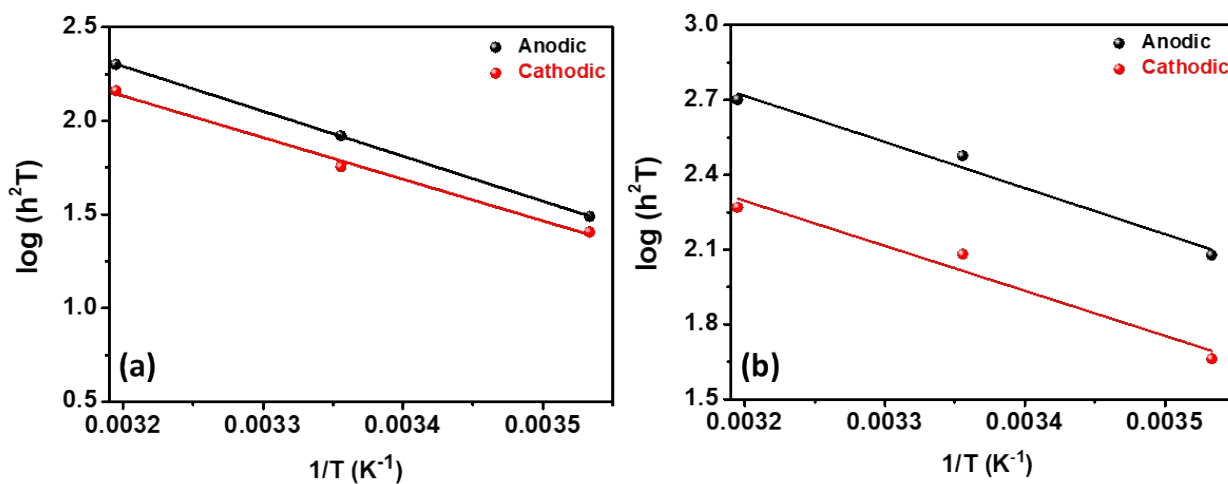


Fig. S16. Plot of the logarithm of (h^2T) against the inverse of temperature for S@NCS and S@NiVP/Pi-NCS respectively in 2 M aq. Na_2SO_4 electrolyte, CE: stainless steel (SS 316), RE: Ag/AgCl/3 M KCl.

Table S2: Comparison of the activation energy (E_a) calculated by combining Randel Sevic equation with Arrhenius plot.

Anode	slope		E_a (Kj mol ⁻¹)	
	Anodic	cathodic	Anodic	cathodic
S@NCS	2400	2233	46.0	42.54
S@NiVP/Pi-NCS	1846	1801	35.35	34.484

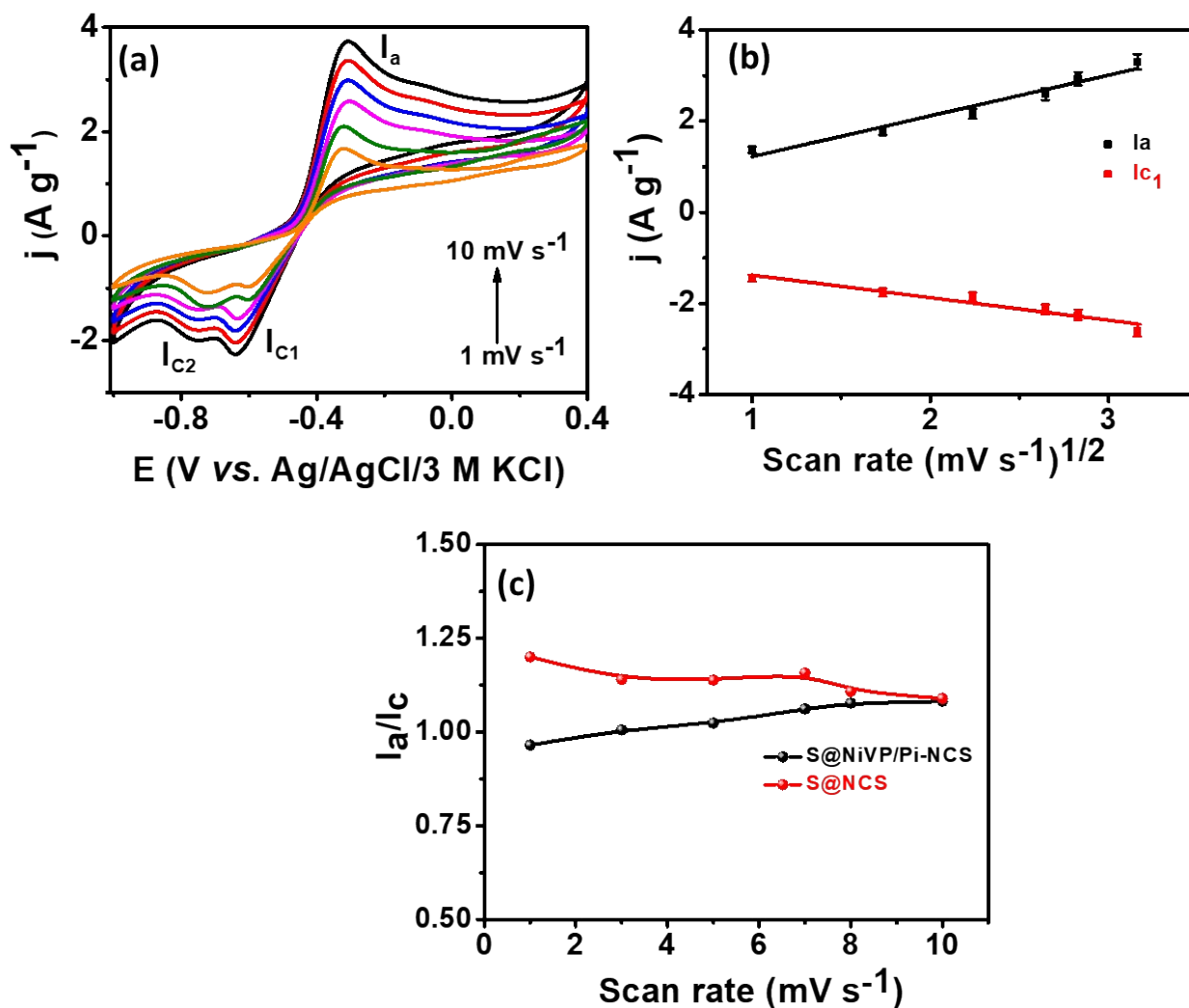


Fig. S17. (a) Cyclic voltammograms at various scan rates, (b) Plot of anodic peak current (I_a) density and cathodic peak current density (I_c) versus square root of scan rate, (c) plot of the ratio of anodic to cathodic density for S@NiVP/Pi-NCS and S@NCS vs. scan rates.

The theoretical capacity of S anode:

$$Q (\text{Ah/g}) = nF/3600 * M.W.$$

n is the number of electrons transfer in the reaction (2),

F is the Faraday constant (96485),

$M.W.$ is molecular weight (S+H₂O) (50)

$$Q = 2 * 96500 / 3600 * 50$$

$$= 1.072 \text{ Ah/g or } 1072 \text{ mAh/g}$$

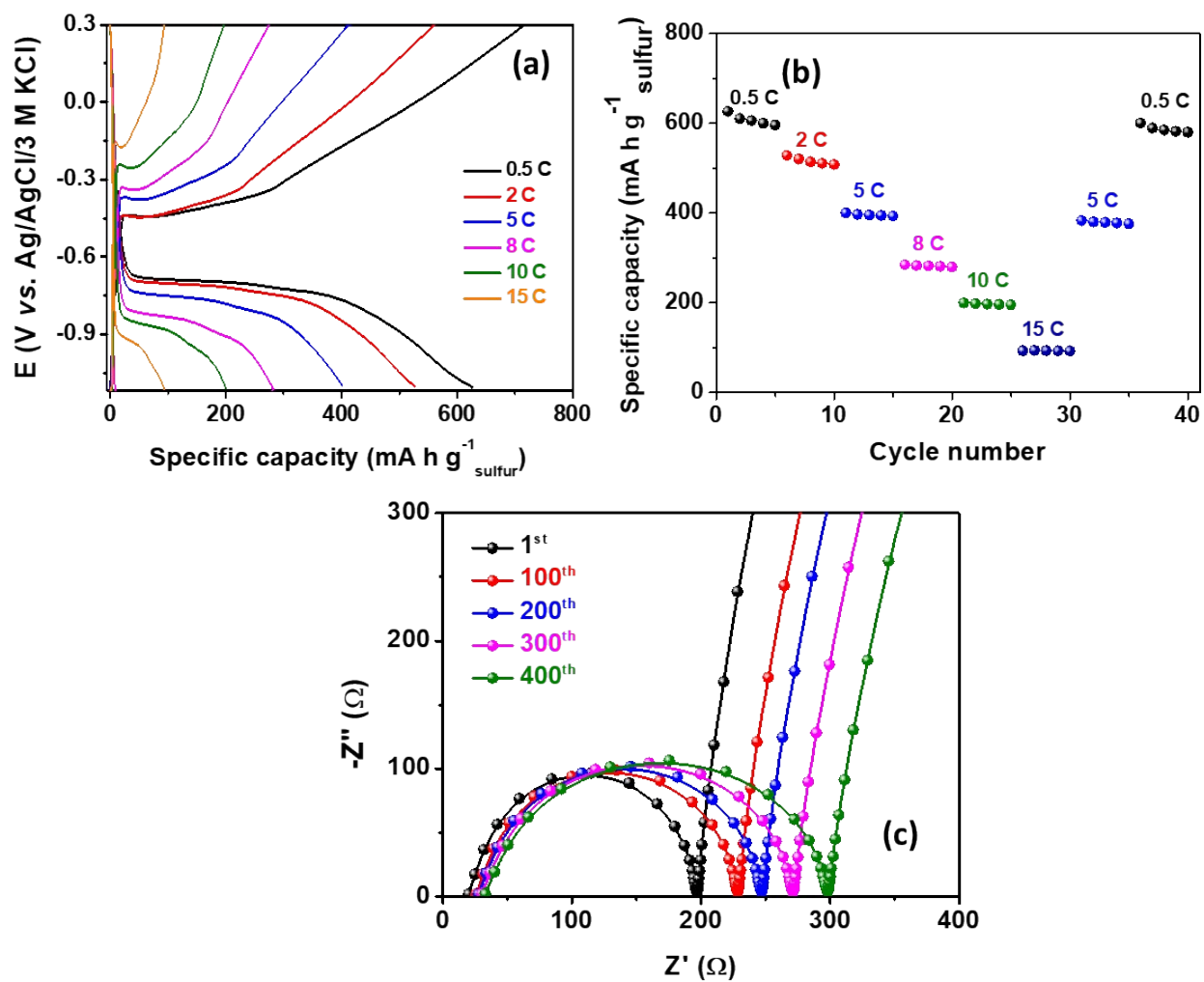


Fig. S18. (a) Galvanostatic charge-discharge curves of S@NCS at various C-rate, (b) rate performance of S@NCS at different C-rate, (c) EIS during cycling performance in 2 M aq. Na_2SO_4 . CE: stainless steel (SS 316), RE: Ag/AgCl/3 M KCl.

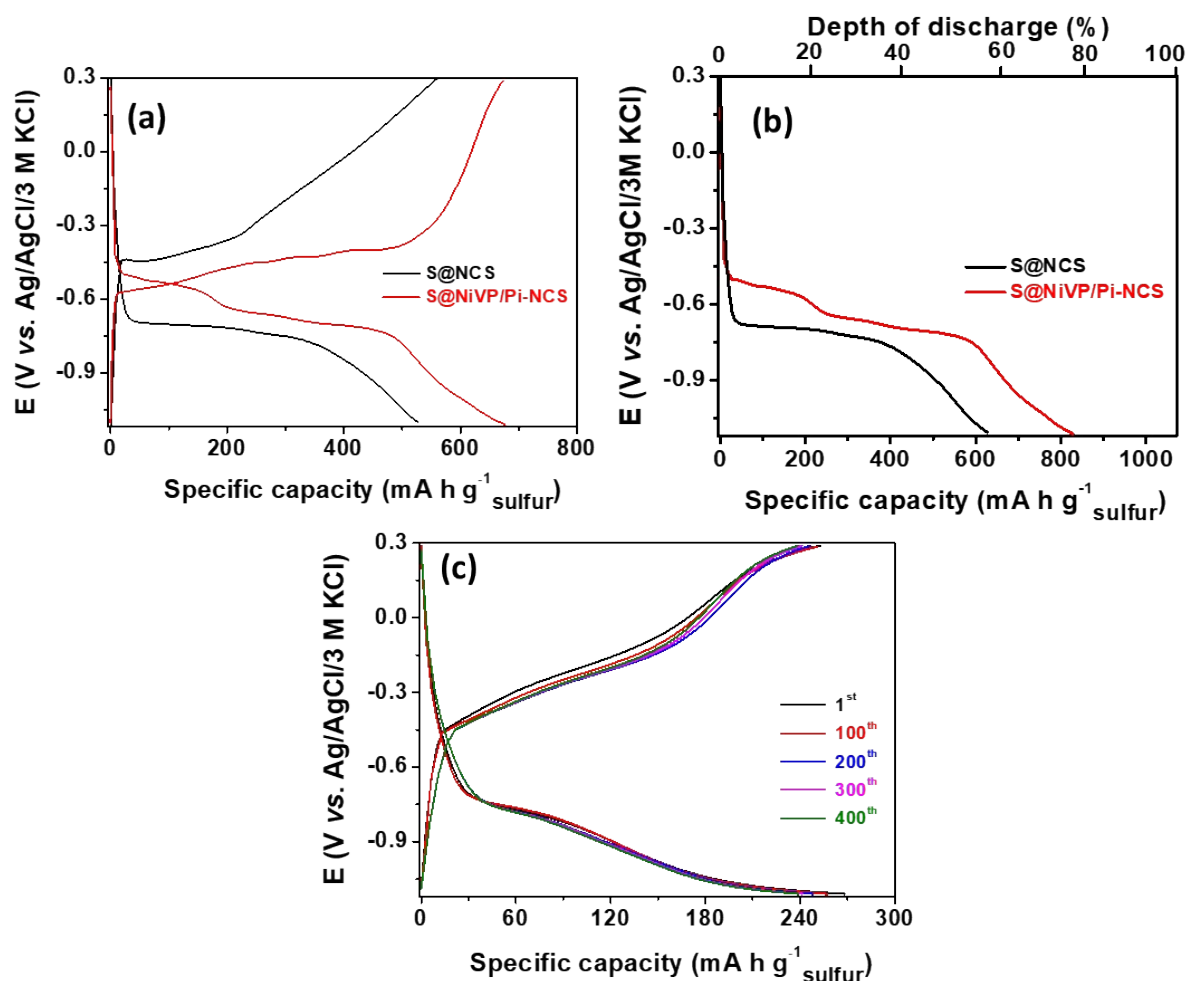


Fig. S19A. (a) Comparative voltage profile for S@NCS and S@NiVP/Pi-NCS at 2 C, and (b) at 0.5 C along with the depth of discharge, and (c) galvanostatic charge-discharge curves of S@NiVP/Pi-NCS at 10 C over 400 cycles in 2 M aq. Na₂SO₄ electrolyte, CE: stainless steel (SS 316), RE: Ag/AgCl/3 M KCl.

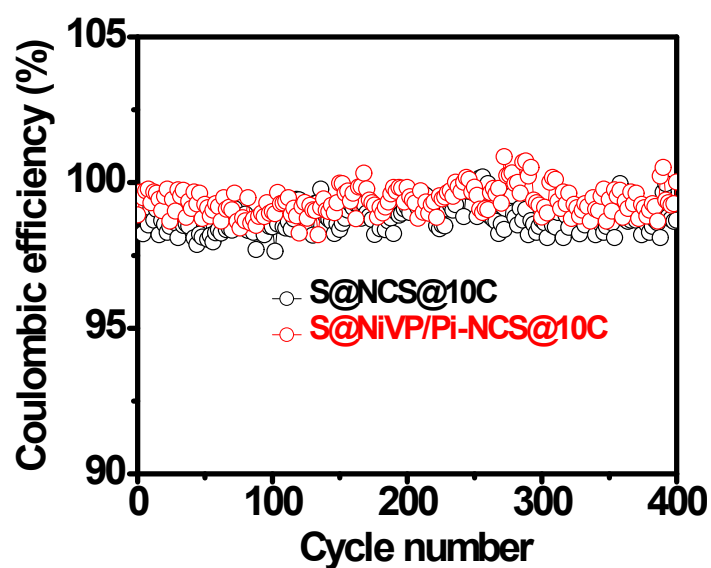


Fig. S19B. Enlargement of Fig. 3h representing the CE of two different anodes @ 10 C.

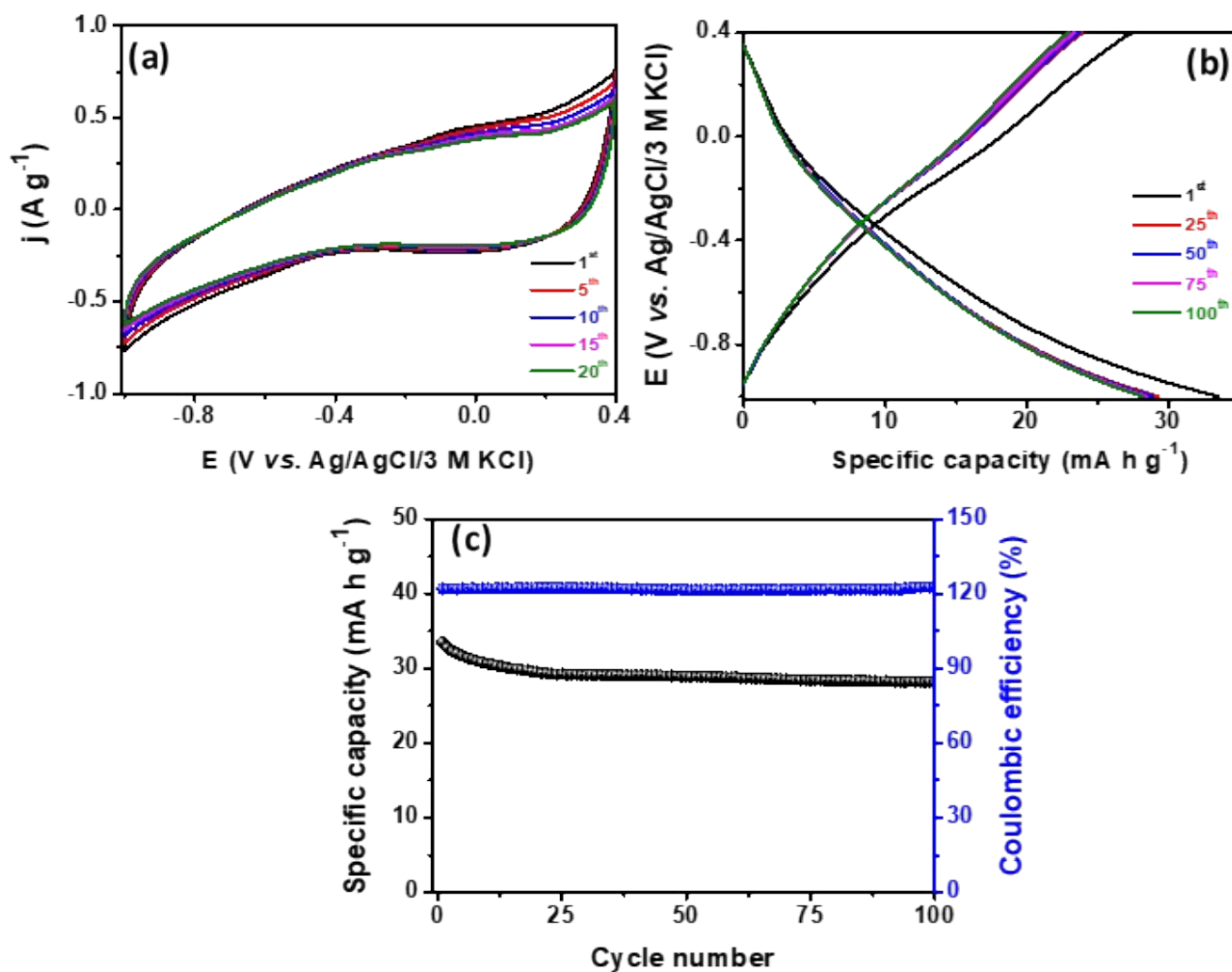


Fig. S20. (a) Cyclic voltammograms of NiVP/Pi at 2 mV s⁻¹ (b) corresponding galvanostatic charge-discharge curves and (c) cycling stability of NiVP/Pi in 2 M aq. Na₂SO₄ electrolyte at 0.5 C, CE: stainless steel (SS 316), RE: Ag/AgCl/3 M KCl.

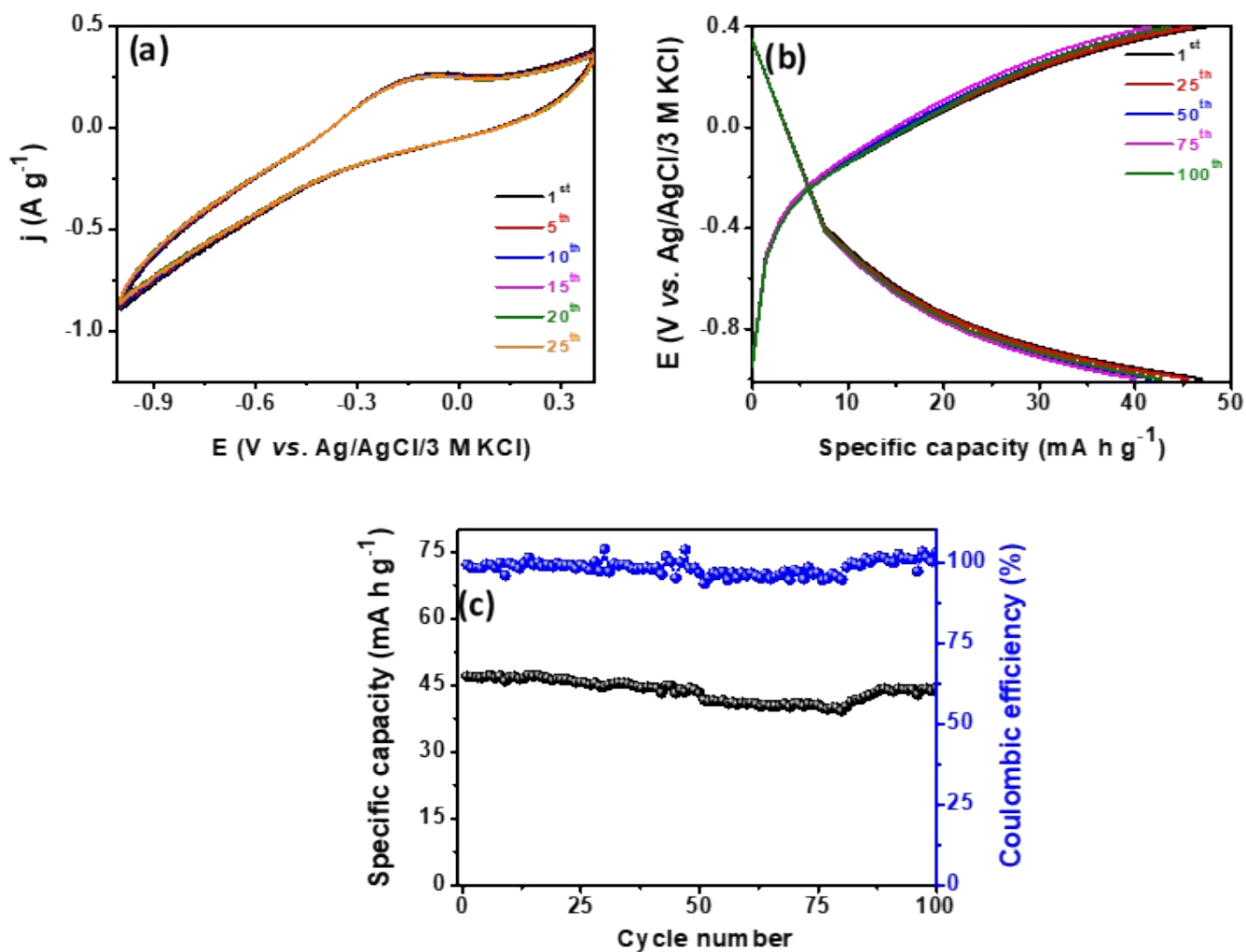


Fig. S21. (a) Cyclic voltammograms of NiVP/Pi-NCS at 2 mV s⁻¹ (b) corresponding galvanostatic charge-discharge and (c) cycling stability of NiVP/Pi-NCS in 2 M aq. Na₂SO₄ electrolyte at 0.5 C, CE: stainless steel (SS 316), RE: Ag/AgCl/3 M KCl.

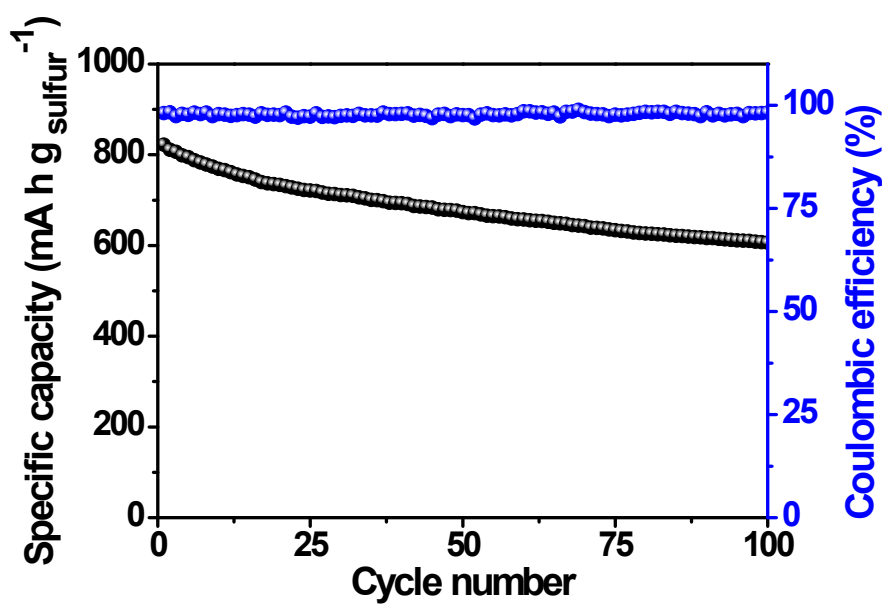


Fig. S22A. Long-term cycling stability of S@NiVP/Pi-NCS anode at 0.5 C over 100 cycles in 2 M aq. Na₂SO₄.

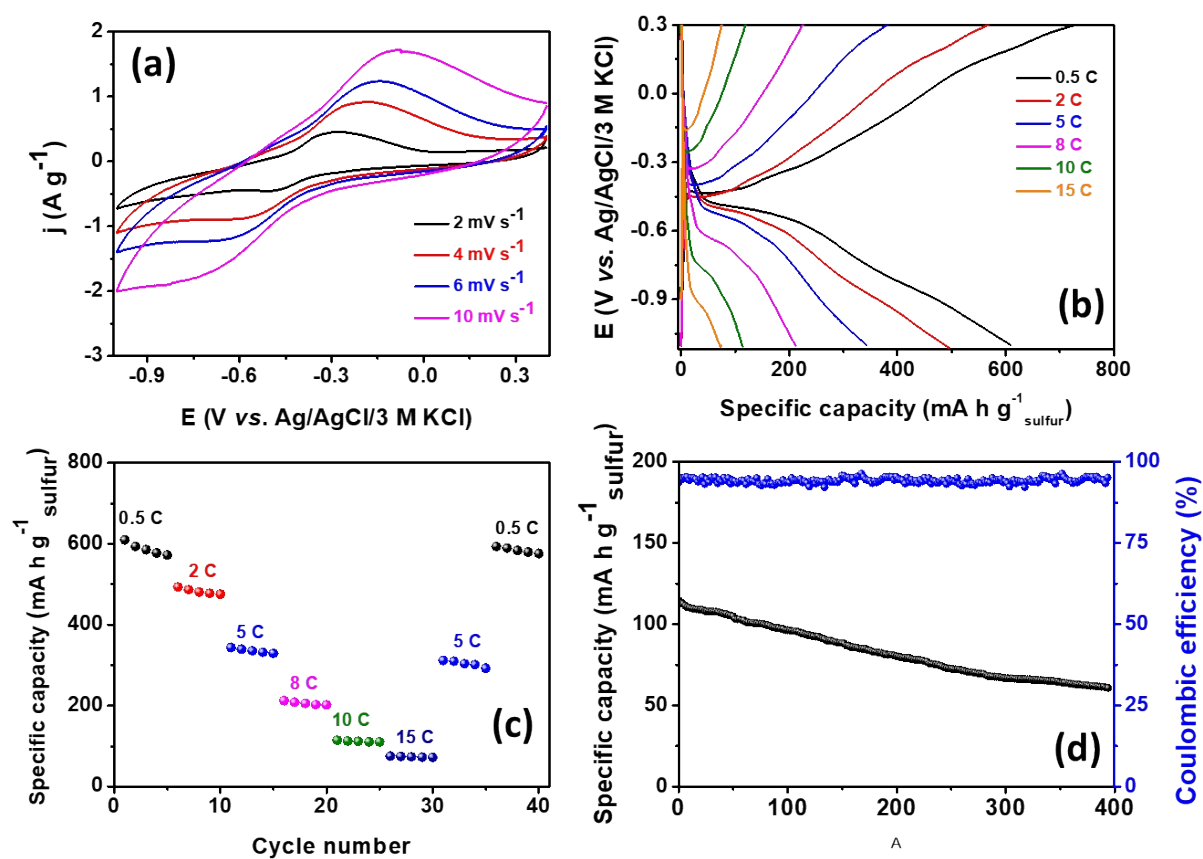


Fig. S22B. (a) Cyclic voltammograms of S@NiP/Pi at various scan rate, (b) voltage profile and (c) rate performance at different C-rates, and (d) long term cycling stability of S@NiP/Pi at 10 C over 400 cycles in 2 M aq. Na₂SO₄ electrolyte CE: stainless steel (SS 316), RE: Ag/AgCl/3 M KCl.

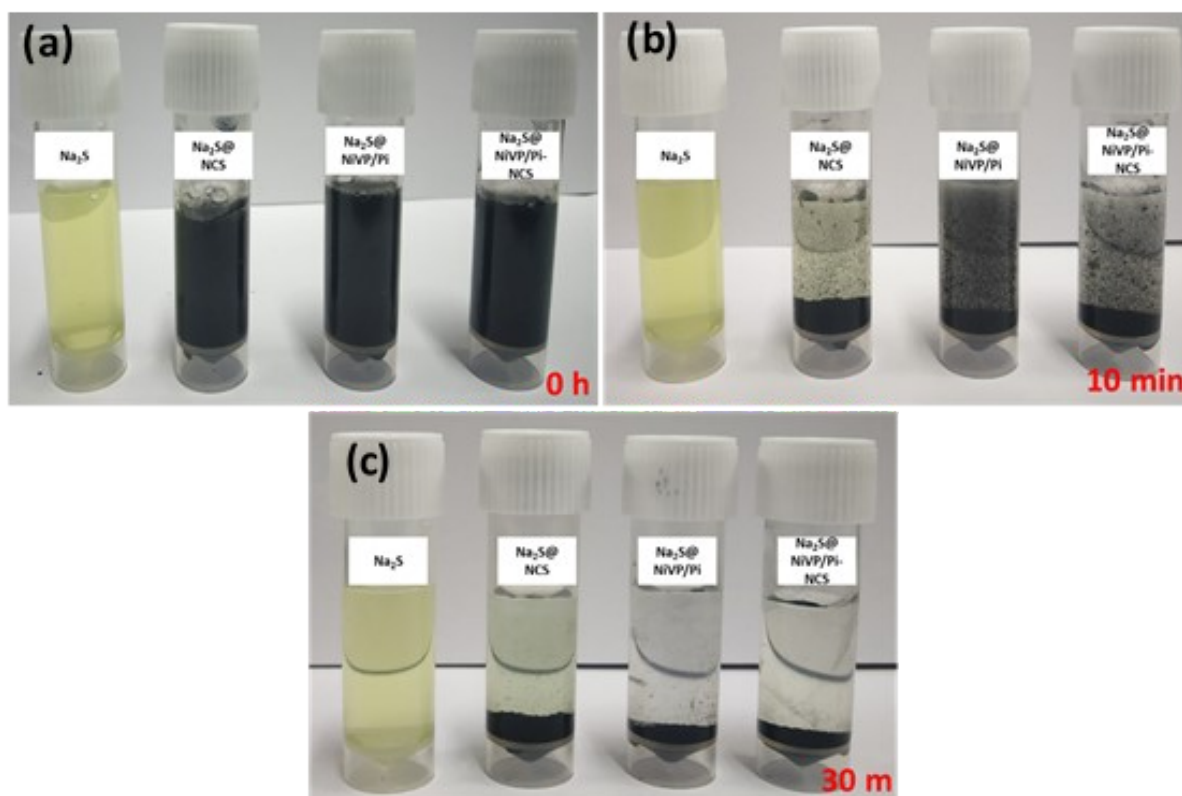
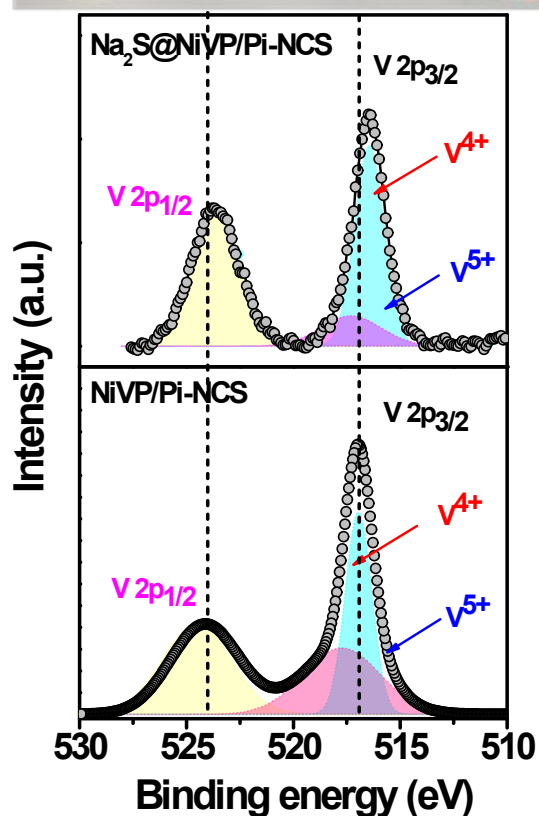


Fig. S23. Optical images of catalyst after (a) 0 min, (b)



Na₂S adsorption test for various 10 min, and (c) 30 mins.

Fig. S24. Deconvoluted XP spectra of V 2p for NiVP/Pi-NCS and Na₂S@NiVP/Pi-NCS.

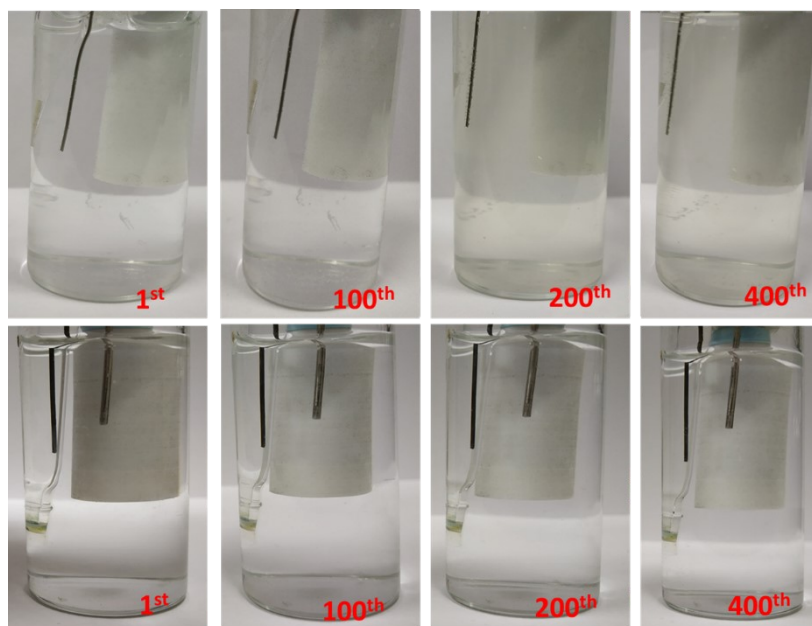


Fig. S25. (a) and (b) are the Optical images of 2 M aq. Na₂SO₄ electrolyte after 1st, 100th, 200th and 400th cycles for S@NCS and S@NiVP/Pi-NCS respectively during battery performance, CE: stainless steel (SS 316), RE: Ag/AgCl/3 M KCl.

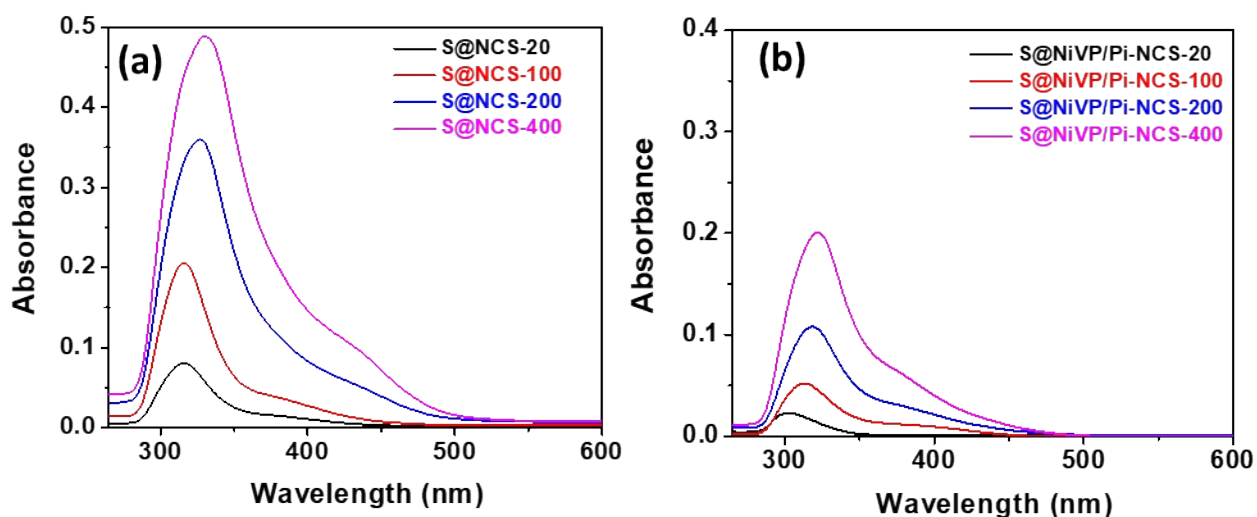


Fig. S26. UV-Vis spectra of dissolved polysulfide in 2 M aq. Na_2SO_4 using (a) S@NCS and (b) S@NiVP/Pi-NCS anode after a various galvanostatic charge-discharge cycles.

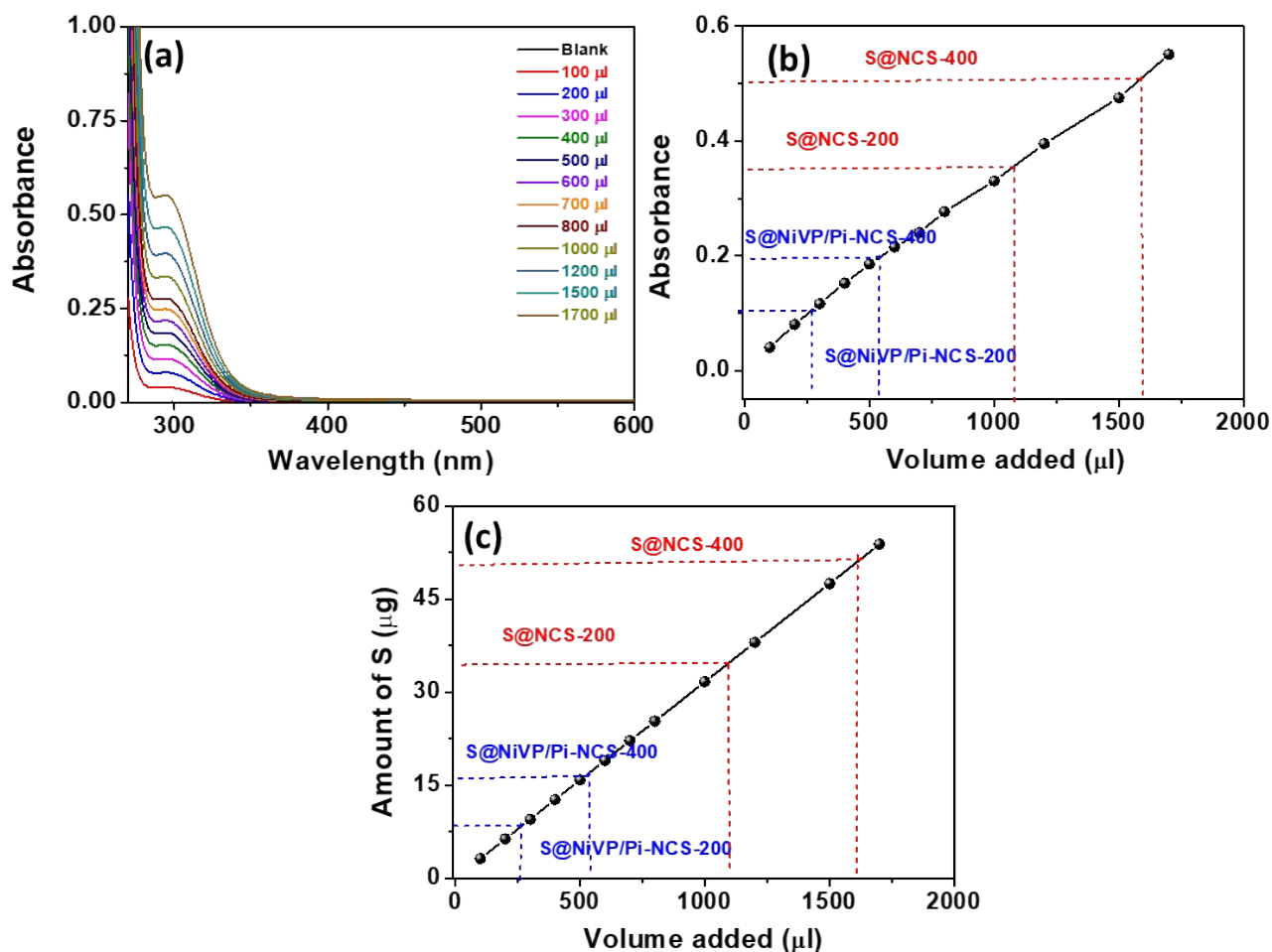
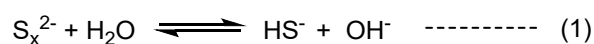


Fig. S27. (a) UV spectra of 2 M aq. Na_2SO_4 electrolyte with various Na_2S concentration (b) plot of absorbance against the amount of Na_2S and (c) is a plot of amount of S against the volume of Na_2S added.

Monitoring the pH of electrolyte during battery performance:

During the electrochemical performance, discharge products can diffuse from electrode surface to electrolyte solution that can alter the pH of the electrolyte. Therefore, keeping the track on the pH of electrolyte during cycling indirectly provides us valuable information about electrode performance. The pH variation of the electrolyte was monitored during the battery performance for both the anodes and tabulated in Table S3 . As observed from Table S3, a clear shift in pH of electrolyte with an increase in the no. of cycle and shift in the values is more for S@NCS compared to S@NiVP/Pi-NCS. This pH shift can be explained based on the dissolution of polysulfides, which immediately leads to the formation of H₂S and make the electrolyte acidic indeed as depicted by the following equation .³



This pH shifts will lead to facile side reactions like HER due to water dissociation and H⁺, it can intercalate with Na⁺, leading to a drastic decrease in the electrode performance. It is noteworthy to mention that there is no drastic change in the pH of both the electrolyte, which confirms significantly less amount of discharge product is able to diffuse out of electrode surface, showing superior performance of both the electrode.

Table S3: Changes in the pH of electrolyte recorded during cycling for both anodes in 2 M aq. Na₂SO₄

Anode	pH of electrolyte				
	Before cycling	20 th cycle	100 th cycle	200 th cycle	400 th cycle
S@NiVP/Pi-NCS	7.35	7.23	7.12	6.99	6.88
S@NCS	7.35	6.98	6.80	6.23	6.08

electrolyte.

Quantification of lost S in the form of polysulfide by UV:

To calculate the lost S in the form of polysulfide, we have initially prepared 1 mM of Na₂S solution and measure the UV spectra by increasing the quantity of Na₂S from 100 – 1700 μl by maintaining the total

volume of reaction to be 3 mL (Fig. S23a). Then we plot the peak value of the absorbance against the volume of Na₂S added (Fig. S23b). Then we simply determine the concentration of Na₂S, by using the molality equation.

Let us consider we added 100 μ l of 1 mM of Na₂S

In that case,

$$M_1V_1 = M_2V_2$$

$$0.001\text{M} \times 0.100 \text{ mL} = M_2 \times 3 \text{ mL}$$

$$M_2 = 33.3 \text{ } \mu\text{M}$$

Further, obtained molarity was used to calculate the weight of Na₂S:

$$0.033 \text{ mM} = x \times 1000 / (78 \times 3)$$

$$x = 7.72 \text{ } \mu\text{g}$$

$$\text{Amount of S in Na}_2\text{S} = 7.72 \times 32 / 78 = 3.16 \text{ } \mu\text{g}$$

Now to calculate the amount of S lost in the form of polysulfide for S@NiVP/Pi-NCS after 400 cycles.

We put the value of absorbance peak in the linear plot and calculate the volume of Na₂S and from their concentration and ultimately loss of S.

Absorbance peak corresponds to 535 μ l of 1 mM Na₂S volume

Therefore, Molarity of Na₂S = 180 μ M

$$\text{Weight of Na}_2\text{S} = 42.12 \text{ } \mu\text{g}$$

$$\text{Amount of S in Na}_2\text{S} = 69.72 \times 32 / 78 = 17.3 \text{ } \mu\text{g}$$

Initial loading of S = 200 μ g

Loss of S in the form of polysulfide = 17.3 μ g

Total loss of S = 8.65 %

Similarly, we determine the loss of S for other anode and cycle no. in table S4

Table S4: Quantification of the amount of S lost in the form of polysulfide by UV spectroscopy

Catalyst	S lost after 200 cycles	S lost after 400 cycles
S@NiVP/Pi-NCS	4.21	8.65
S@NCS	17.12	27.2

Potentiometric titration:

It is essential to determine loss of active to understand the performance of electrode material. Therefore, we carried out a potentiometric titration method to estimate the loss of sulfur in the form of sodium

polysulfide. For that, titration was carried out using 5 mM $\text{Pb}(\text{NO}_3)_2$ as a titrating agent and Pb/PbS as a sensor electrode. To estimate the amount of S, 3 mL sodium polysulfide solution obtained after the galvanostatic charge-discharge at 10 C was titrated with 5 mM $\text{Pb}(\text{NO}_3)_2$, and observed potentials were plotted against the volume of $\text{Pb}(\text{NO}_3)_2$ to estimate the amount of lost S. The obtained results show that S@NCS shows 30.2 % loss of S after 400 cycles. In contrast, the S@NiVP/Pi-NCS indicates only 16.24 % loss of S after 400 cycles at 10 C by taking the first derivative endpoint of the reaction was determined.

For S@NiVP/Pi-NCS after 400 cycles:

The potentiometric titration follows the following reaction pathway



By using the molarity equation, the molarity of the Na_2S was determined,

$$M_1V_1 = M_2V_2$$

$$0.005\text{M} \times 0.203 \text{ mL} = M_2 \times 3 \text{ mL}$$

$$M_2 = 0.34 \text{ mM}$$

Further, obtained molarity was used to calculate weight of Na_2S :

$$0.34 \text{ mM} = x \times 1000 / (78 \times 3)$$

$$x = 79.17 \text{ } \mu\text{g}$$

$$\text{weight of S in Na}_2\text{S} = 79.17 \times 32 / 78 = 32.48 \text{ } \mu\text{g}$$

$$\text{Initial loading of S} = 200 \text{ } \mu\text{g}$$

$$\text{Loss of S in form of polysulfide} = 32.48 \text{ } \mu\text{g}$$

$$\text{Total loss of S} = 16.24 \%$$

Similarly, we determine the loss of S for S@NCS after 400 cycle equivalents to 30.2 %.

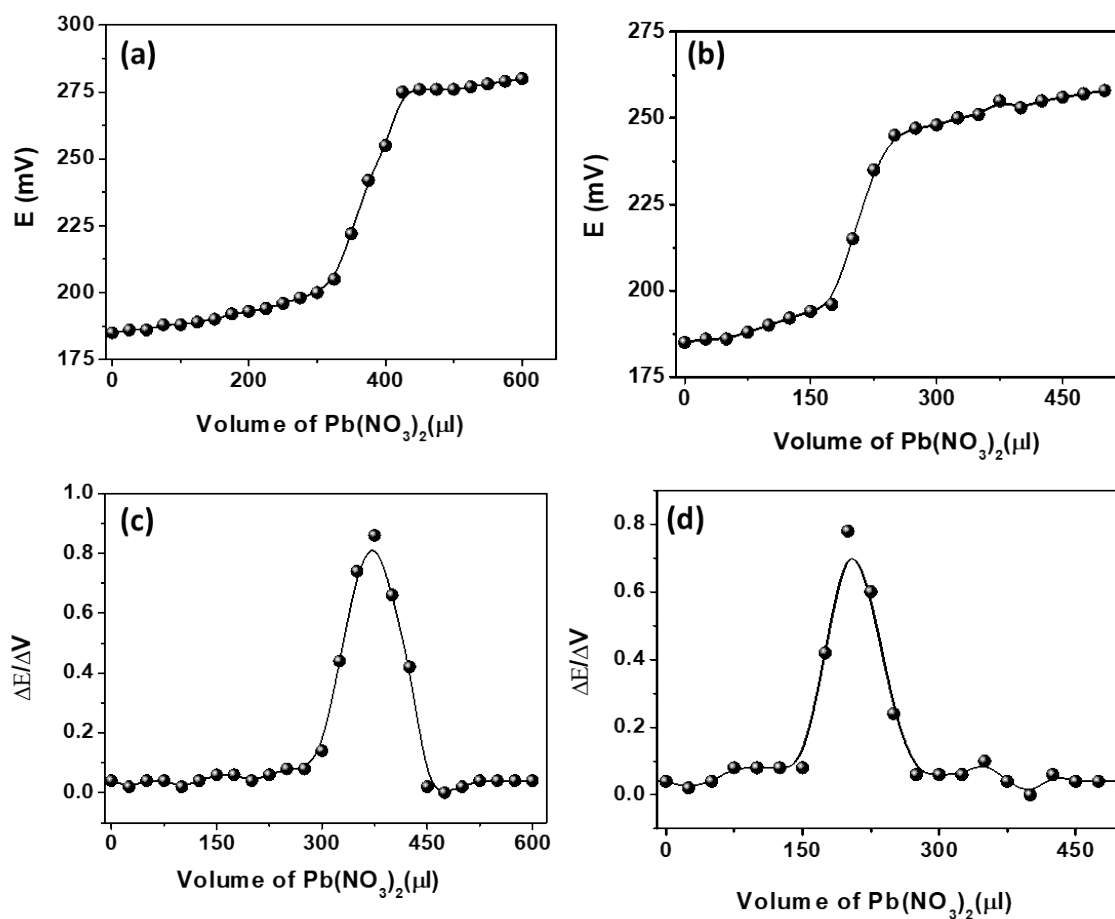


Fig. S28.(a) and (b) are the potentiometric titration curve and (c) and (d) its corresponding first-order derivative plot for sodium polysulfide in 2 M aq. $NaClO_4$ electrolyte after 400 cycles for S@NCS and S@NiVP/Pi-NCS anode using PbS as sensor electrode and 1 mM $Pb(NO_3)_2$ as a titrating agent.

Table S5: Quantification of the amount of S lost in the form of polysulfide during cycling by potentiometric titration.

Catalyst	S lost after 400 cycles
S@NCS	16.24
S@NiVP/Pi-NCS	30.2

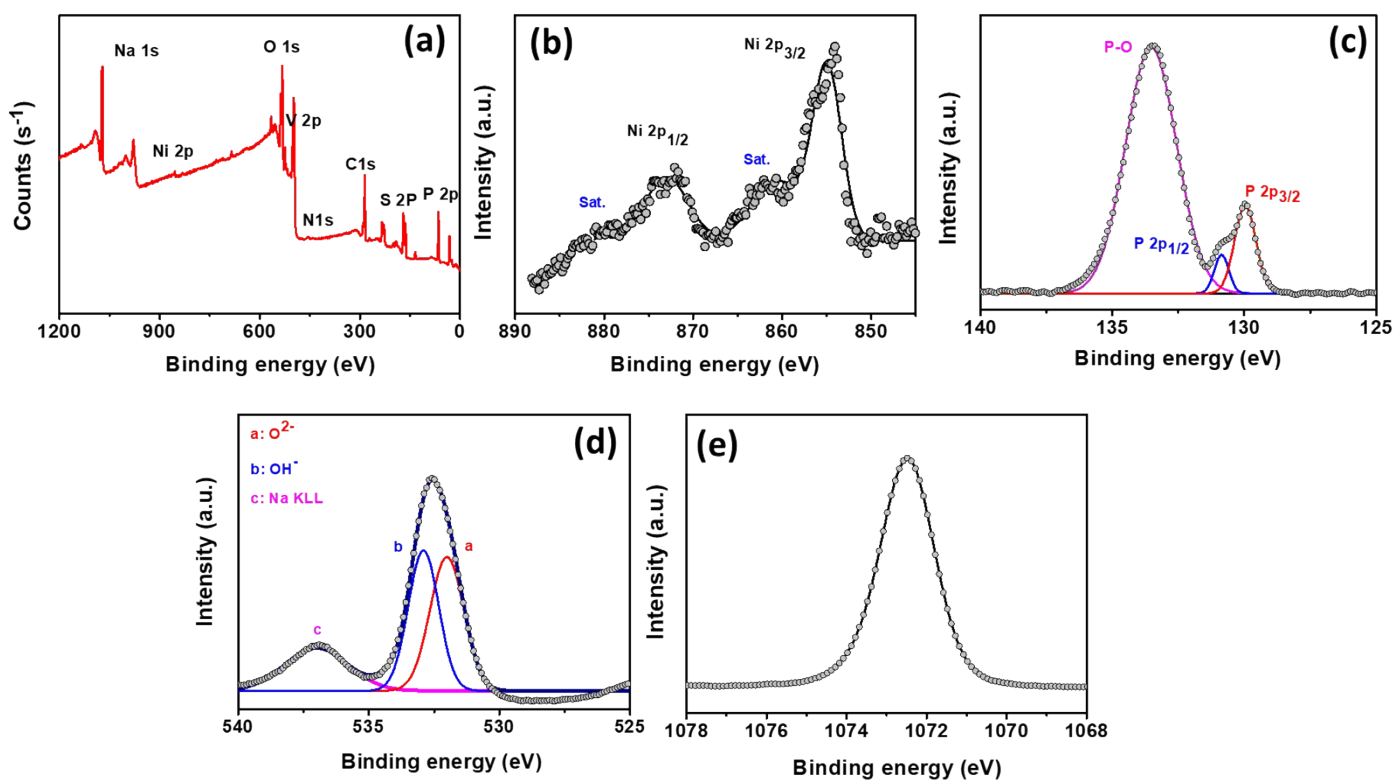


Fig. S29. (a) XPS survey spectra, deconvoluted XP spectra for (b) Ni 2p, (c) P 2p, (d) O 1s, and (e) Na 1s of S@NiVP/Pi-NCS anode after charging process.

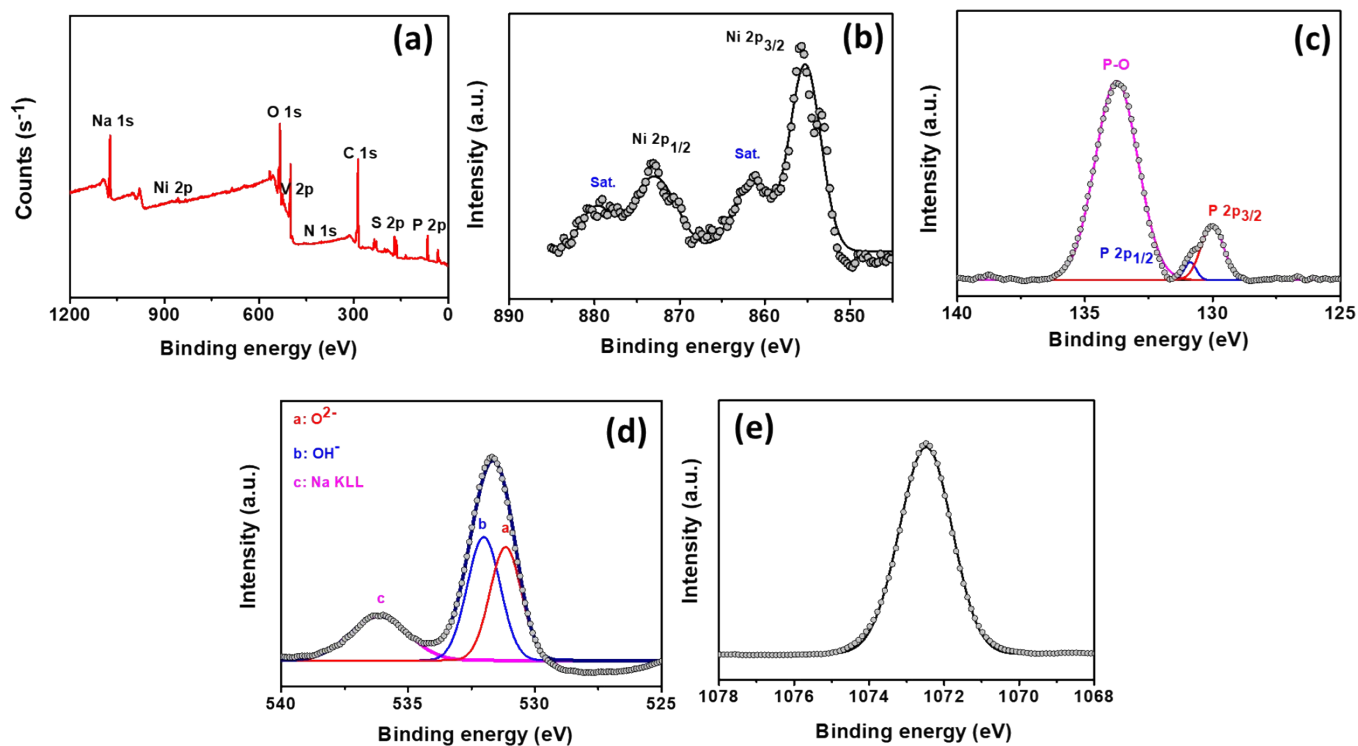


Fig. S30. (a) XPS survey spectra, deconvoluted XP spectra for (b) Ni 2p, (c) P 2p, (d) O 1s, and (e) Na 1s of S@NiVP/Pi-NCS anode after discharging process.

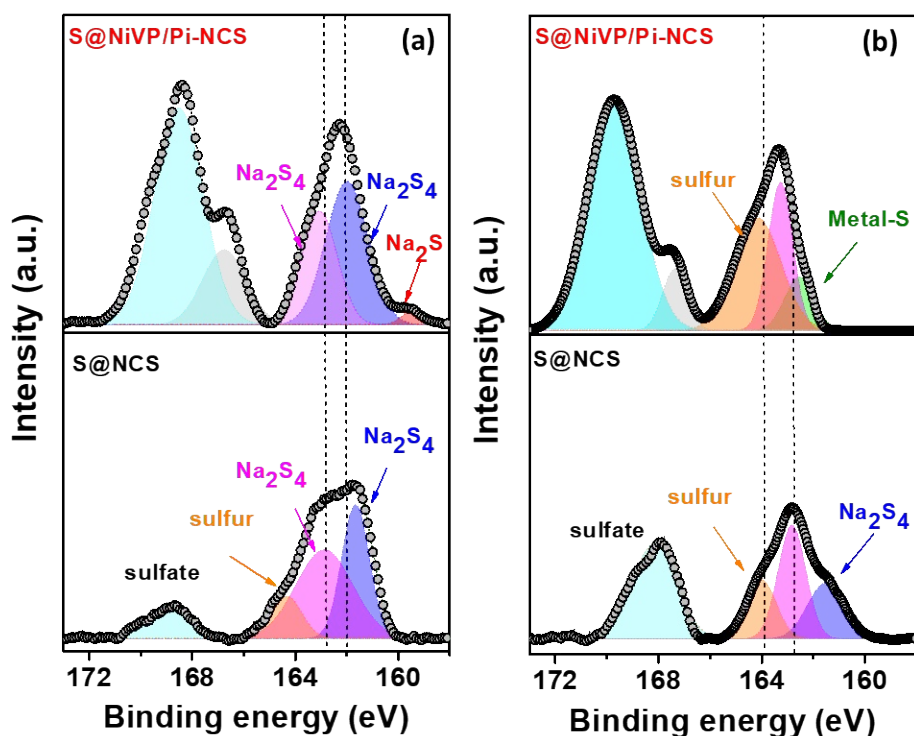


Fig. S31. Deconvoluted S 2p XP spectra for S@NCS and S@NiVP/Pi-NCS after (a) discharging and (b) after charging.

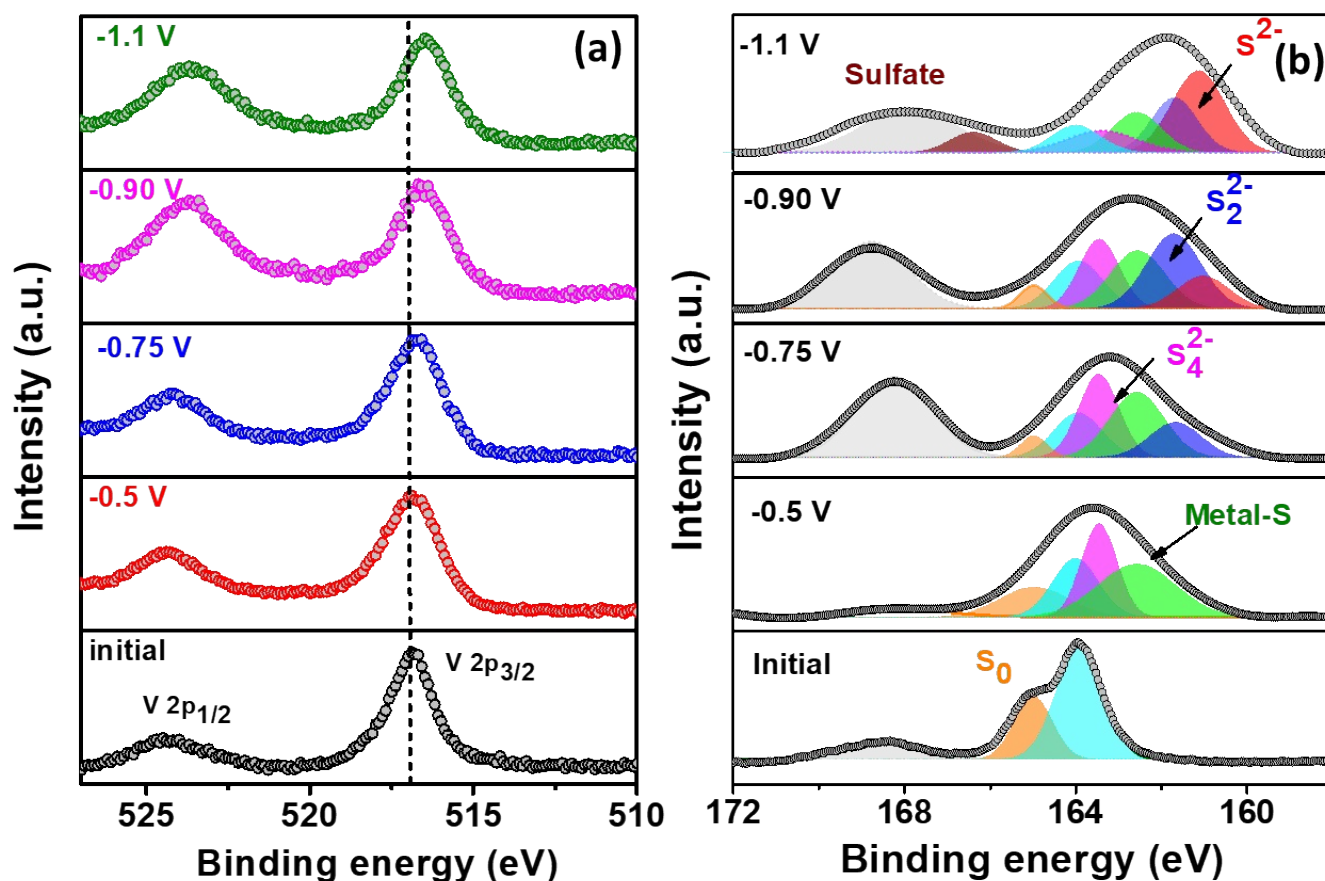


Fig. S32. Deconvoluted XP spectra of (a) V 2p and (b) S 2p of S@NiVP/Pi-NCS anode at various potentials during discharging process.

To understand the polysulfide formation the XPS analysis of the retrieved anode were performed at different discharge potentials for S@NiVP/Pi-NCS. Before applying potential, a pair of peaks at 164.9 eV and 164.0 eV were observed due to elemental sulfur. At -0.5 V the elemental sulfur peaks started to diminish, and additional peaks due to metal sulfide (162.7eV and 163.7 eV) and a peak at 163.5 eV due to the presence of intermediate polysulfide (Na_2S_x , $X=4-8$) appeared. On sweeping the potential to -0.75 V, elemental S peaks keep on diminishing and a new peak at 163.0 eV was observed corresponding to Na_2S_4 along with an additional peak at 161.7eV due to Na_2S_2 . Further at -0.90 V, both S and Na_2S_4 peaks were diminished and the peak at 161.0 eV (Na_2S_2 and Na_2S) became prominent. At -1.1 V, the peaks for elemental S and Na_2S_4 disappeared and the peak due to Na_2S became the most prominent. While in V 2p XP spectra, BE continuously shifted to a lower value during a discharge, once again confirming the significant role of the NiVP/Pi catalysts in accelerating the polysulfide redox kinetics. More importantly, the NiVP/Pi introduction increases anchoring ability and helps to catalyse the polysulfide redox kinetics by lowering the energy barrier and improving the sulfur utilization.

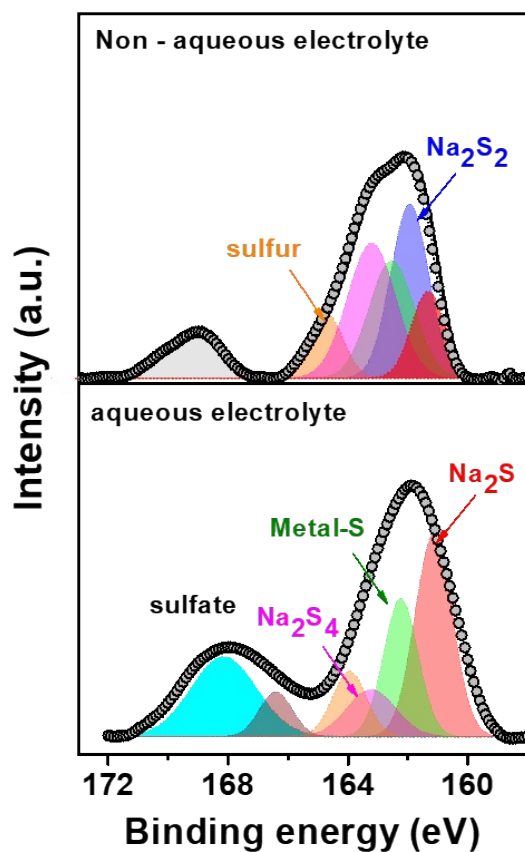


Fig. S33A. Deconvoluted XP spectra of S 2p after 100 % discharge for S@NiVP/Pi-NCS in both aqueous and non-aqueous electrolytes.

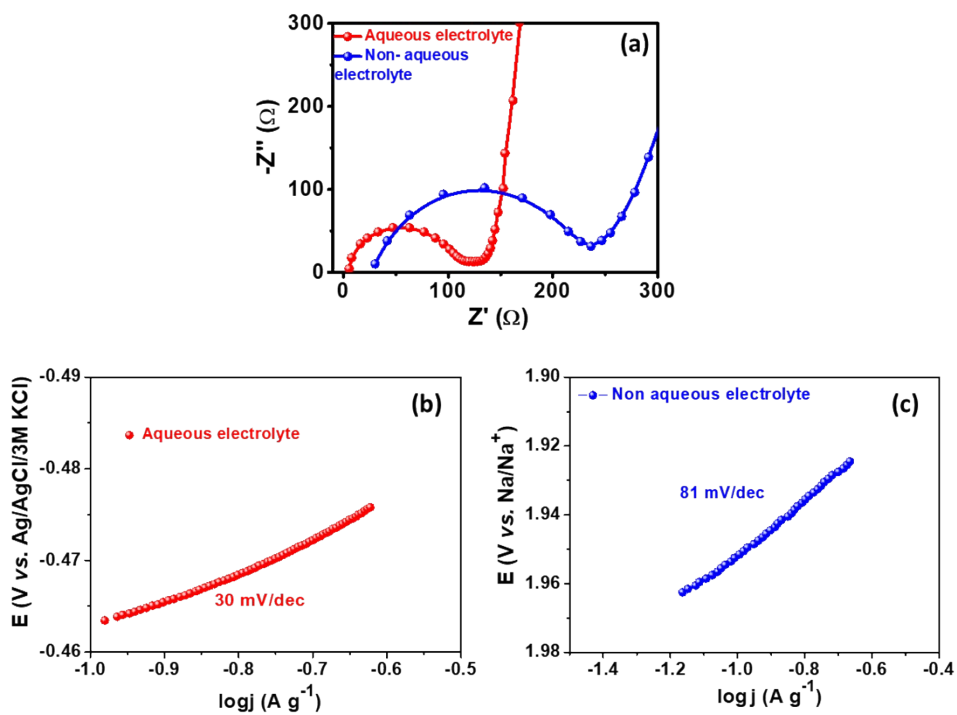


Fig. S33B. (a) EIS (b) and (c) are Tafel slope for S@NiVP/Pi-NCS anode in aqueous electrolyte and non-aqueous electrolyte respectively.

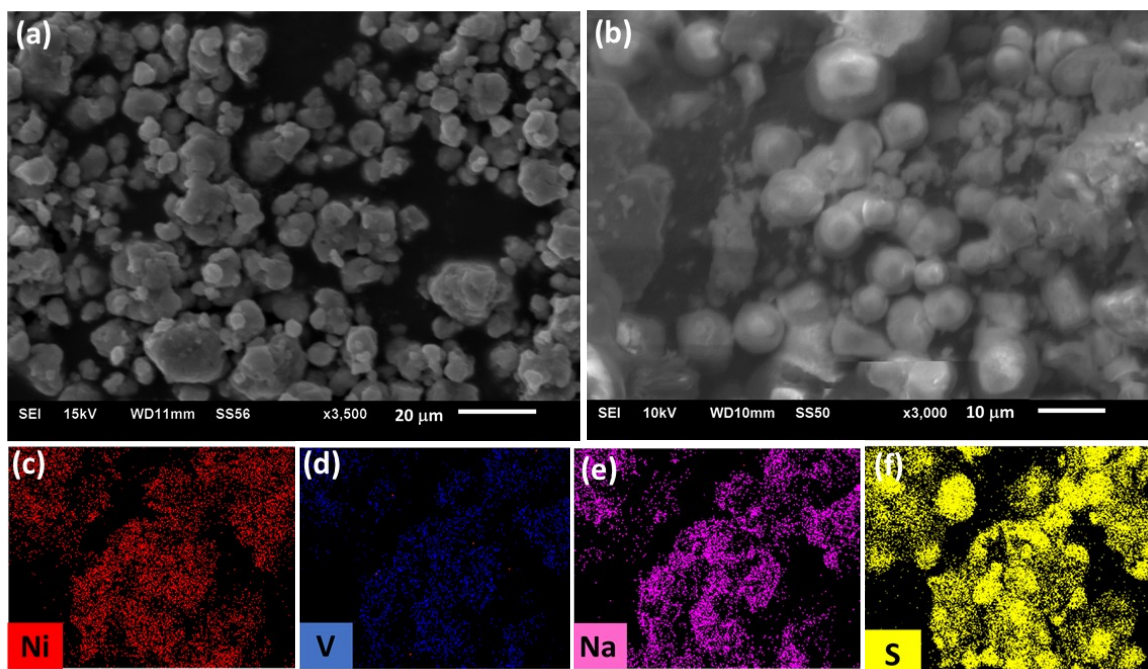


Fig. S34. (a) and (b) SEM images of S@NiVP/Pi-NCS at different magnification after cycling stability, and corresponding EDS elemental dot mapping images of (c) nickel, (d) vanadium, (e) sodium, and (f) sulfur.

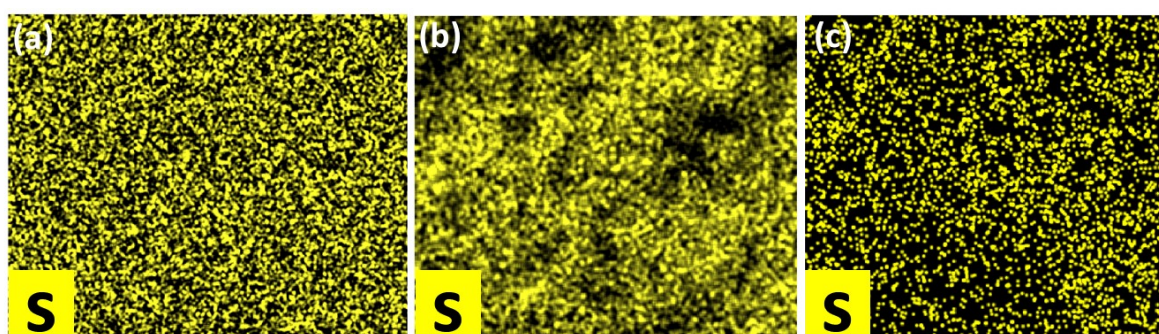


Fig. S35. Elemental dot mapping images of sulfur in S@NiVP/Pi-NCS (a) initially, (b) after discharging and (c) charging.

Osmotic pressure test:

During battery performance, especially in sulfur-based batteries separator plays a crucial role. The most commonly used celgard separator unavoidably allows the passage of dissolved polysulfide from anode to cathode side and retard the cycling stability of the cell. Conversely, negatively charged membranes (SO_3 groups) supposed to inhibit polysulfide dissolution. In order to assure restricted polysulfide shuttling, the polysulfide dissolution experiments were first conducted to understand the polysulfide leakage through the membrane. To perform these tests, different concentrations of polysulfides (Na_2S_2) were dissolved in 2 M Na_2SO_4 and placed in a glass vial whose cap has a small hole covered with a Nafion membrane with the help of an o-ring. Then, these polysulfide-containing vials were inverted into 2 M Na_2SO_4 aqueous electrolytes. As shown in Fig. 5a-5c, three different concentrations *viz.* 2 M, 1 M, 0.5 M of polysulfide was added to 2 M Na_2SO_4 to obtain a final concentration of 4 M, 3 M and 2.5 M inside a small vial which creates a concentration gradient between two sides. As anticipated, due to the repulsion between negatively charged membranes (SO_3 groups) and negatively charged polysulfide, we did not observe any leakage of the polysulfide even after 20 days. Hence, these results depicted that even if the polysulfide diffused from the electrode surface the Nafion membrane guaranteed that polysulfide do not shuttle from anode to cathode.

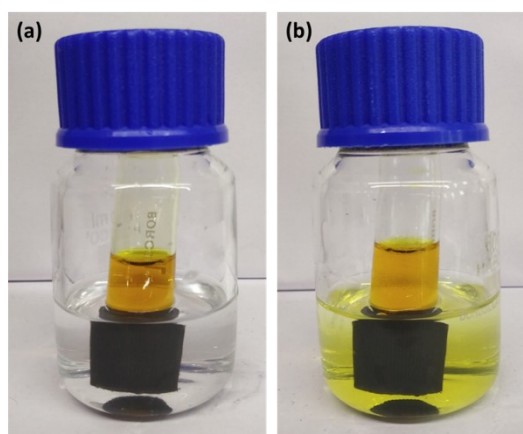


Fig. S36. Photographic images of polysulfide leakage test after 2 days for (a) Nafion membrane and (b) Celgard 2400 PP separator by dissolving 0.5 M polysulfide in 2 M Na_2SO_4 aqueous electrolyte in vial and then placed in a 2 M Na_2SO_4 in water.

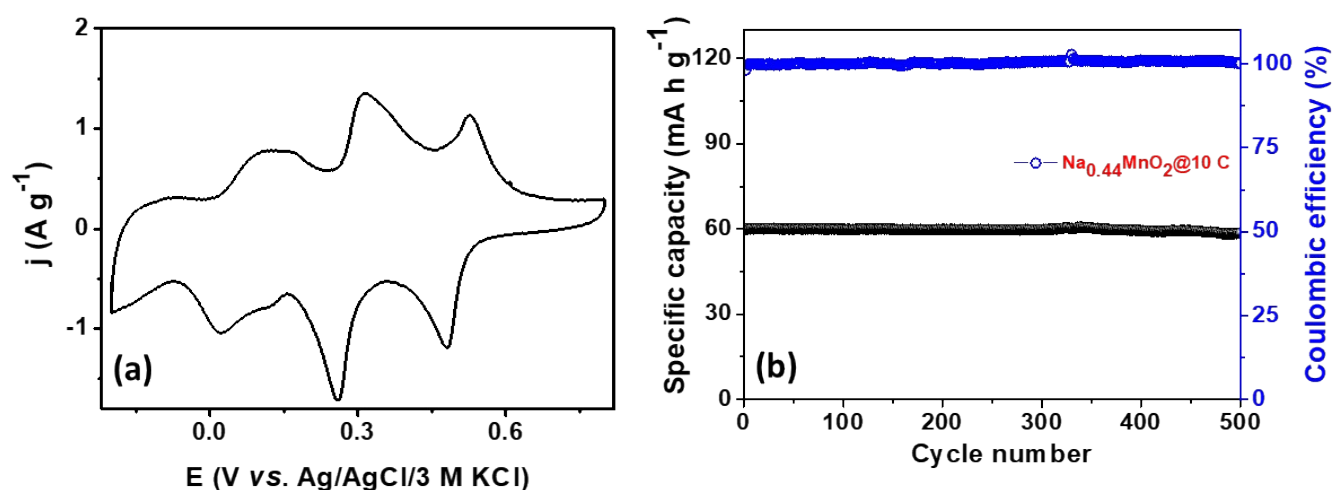


Fig. S37. (a) Cyclic voltammograms, (b) long-term cycling performance of $\text{Na}_{0.44}\text{MnO}_2$ cathode at 10 C in 2 M aq. Na_2SO_4 , CE: stainless steel (SS 316), RE: Ag/AgCl/3 M KCl.

The cyclic voltammogram at 2 mV s^{-1} shown in Fig. S37, for $\text{Na}_{0.44}\text{MnO}_2$ reveals three clear oxidation and reduction peaks in the potential range between -0.2 V to 0.8 V without the dissociation of water. These three redox peaks could be attributed to the multiphase transition mechanism of Na^+ insertion and de-insertion, which matches well with previously reported literature.

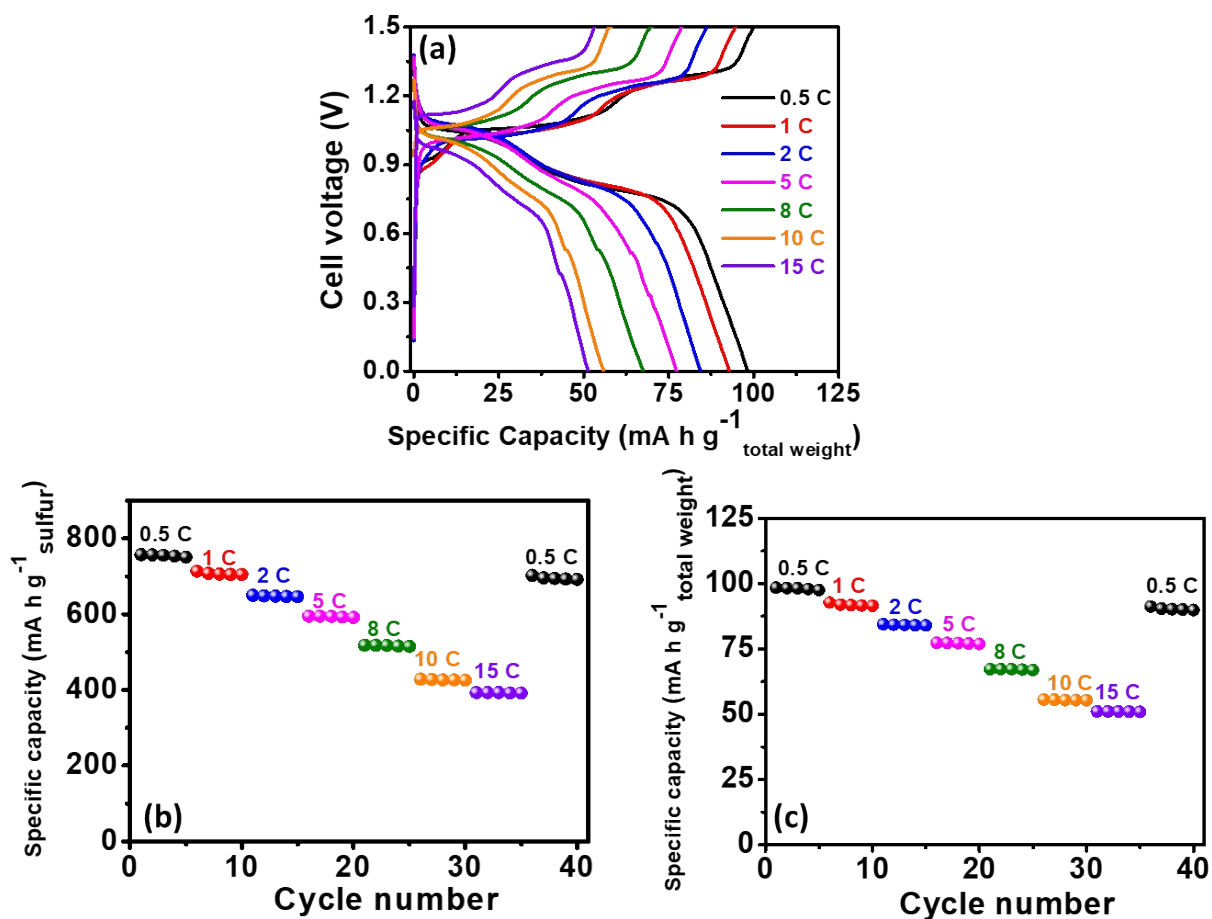


Fig. S38. (a) Voltage profile of full cell battery assembled using S@NiVP/Pi-NCS anode and Na_{0.44}MnO₂ cathode w.r.t total electrode weight, (b) and (c) rate performances at different C-rate w.r.t only sulfur weight and total electrode weight respectively, in 2 M aq. Na₂SO₄. Anode: S@NiVP/Pi-NCS, Cathode: Na_{0.44}MnO₂.

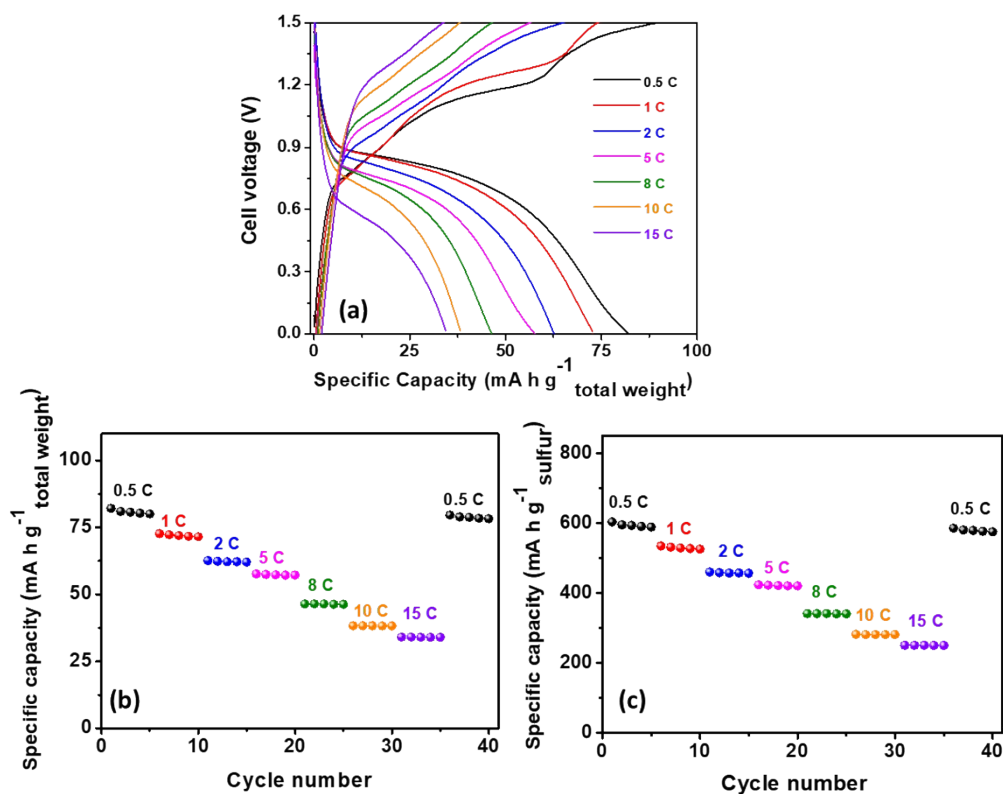


Fig. S39A. (a) Voltage profile of full cell battery assembled using S@NCS anode and Na_{0.44}MnO₂ cathode w.r.t total electrode weight, (b) and (c) rate performances at different C-rate w.r.t only sulfur weight and total electrode weight respectively, in 2 M aq. Na₂SO₄. Anode: S@NCS, Cathode: Na_{0.44}MnO₂.

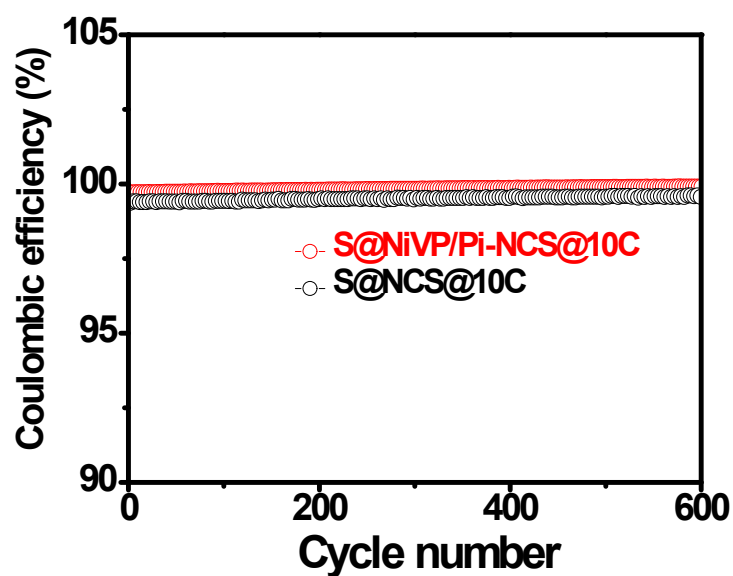


Fig. S39B. Enlargement of Fig. 5f represents the CE of the full cell assembled with two different anodes.

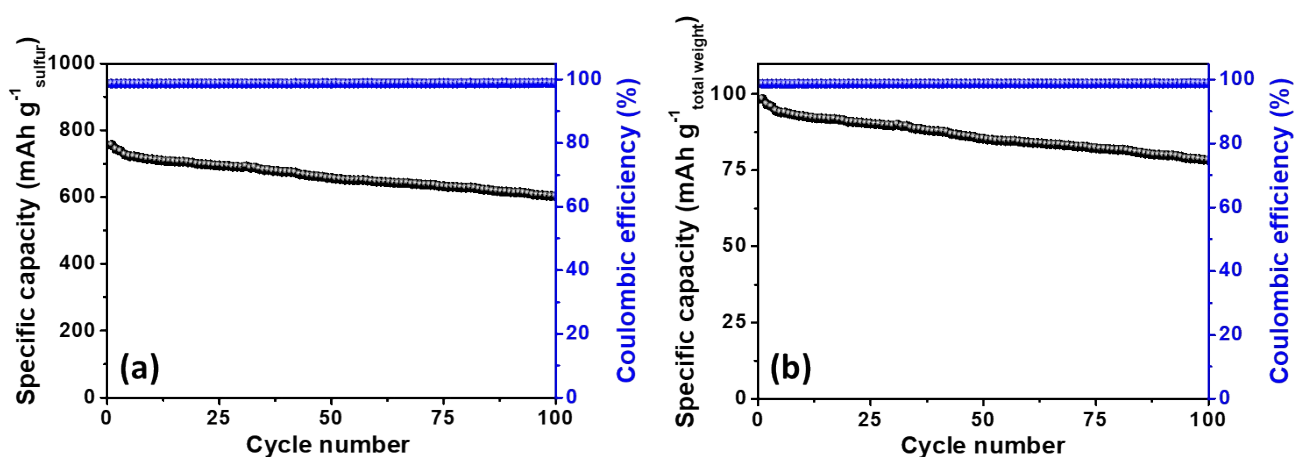


Fig. S40A. Long-term cycling stability of the full cell assembled with S@NiVP/Pi-NCS anode + Na_{0.44}MnO₂ cathode @ 0.5 C based upon (a) sulfur weight only, (b) total electrode weight in 2 M Na₂SO₄ with Nafion membrane.

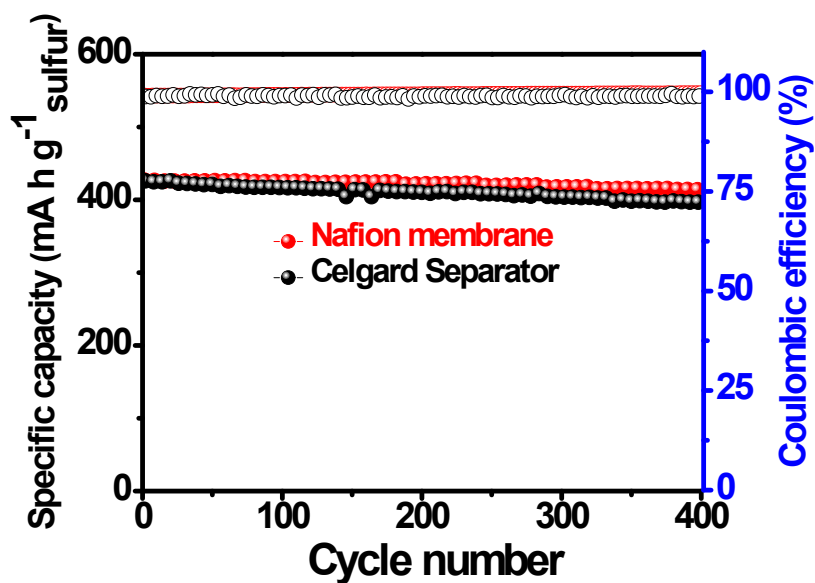


Fig. S40B. Long-term cycling stability of the full cell assembled with S@NiVP/Pi-NCS anode + Na_{0.44}MnO₂ cathode Nafion membrane and celgard separator.

Table S6: Comparison of anode material for aqueous sodium-ion battery

Anode	Cathode	Energy density (Wh kg ⁻¹)	Electrolyte	Ref.
NaTi ₂ (PO ₄) ₃	Na _{0.44} MnO ₂	33	1 M Na ₂ SO ₄	13
WO ₃	KVO _x [Fe(CN) ₆](VHCF)	17	NaClO ₄ +HClO ₄ +PEG	14
NaTi ₂ (PO ₄) ₃	Na _{0.66} [Mn _{0.66} Ti _{0.34}]O ₂	31	9.26 m NaOTF	15
NaTi ₂ (PO ₄) ₃	NaMnO ₂	30	2 M CH ₃ COONa	16
NaTi ₂ (PO ₄) ₃	Na ₂ NiFe(CN) ₆	42.5	1 M Na ₂ SO ₄	17
polyimide–MWCNTs	Na _{0.44} MnO ₂	25	1 M Na ₂ SO ₄	6
NaTi ₂ (PO ₄) ₃	Na ₂ Zn ₃ [Fe(CN) ₆] ₂	55	17 m NaClO ₄	18
S@NiVP/Pi-NCS	Na_{0.44}MnO₂	84	2 M Na₂SO₄	This work

Table S7: Comparison of the energy density of a full cell for ARSIBs

S.No.	Anode materials	Capacity (mAh/g)	Ref.
1.	NaV ₃ (PO ₄) ₃ @C hybrid nanofiber	118 (1C)	4
2.	Self-assembled wafer-like porous NaTi ₂ (PO ₄) ₃	119.4 (1C)	5
3	polyimide–MWCNTs	149	6
4.	Dissolved Polysulfide Na ₂ S ₅	150	7
5.	hydrated FePO ₄	80 (0.5 C)	8
6.	Na ₃ Fe ₂ (PO ₄) ₃	57(2C)	9
7.	TiNb(PO ₄) ₃	119(1C)	10
8.	Na ₂ Ti ₃ /2Mn _{1/2} (PO ₄) ₃	88.6 (0.5 C)	11
9.	Na ₃ MgTi(PO ₄) ₃	54 (0.2 C)	12
10.	S@NCS	626 (0.5 C)	This Work
11.	S@NiVP/Pi-NCS	826 (0.5 C)	This Work

References:

1. J. Zhu, E. Yildirim, K. Aly, J. Shen, C. Chen, Y. Lu, M. Jiang, D. Kim, A. E. Tonelli and M. A. Pasquinelli, *J. Mater. Chem. A*, 2016, **4**, 13572-13581.
2. Y. Tao, Y. Wei, Y. Liu, J. Wang, W. Qiao, L. Ling and D. Long, *Energy Environ. Sci.*, 2016, **9**, 3230-3239.
3. X. Wu, X. Yuan, J. Yu, J. Liu, F. Wang, L. Fu, W. Zhou, Y. Zhu, Q. Zhou and Y. Wu, *Nanoscale*, 2017, **9**, 11004-11011.
4. L. Ke, J. Dong, B. Lin, T. Yu, H. Wang, S. Zhang and C. Deng, *Nanoscale*, 2017, **9**, 4183-4190.
5. B. Zhao, Q. Wang, S. Zhang and C. Deng, *J. Mater. Chem. A*, 2015, **3**, 12089-12096.
6. T. Gu, M. Zhou, M. Liu, K. Wang, S. Cheng and K. Jiang, *RSC adv.*, 2016, **6**, 53319-53323.
7. B. Tekin, S. Sevinc, M. Morcrette and R. Demir-Cakan, *Energy Technol.*, 2017, **5**, 2182-2188.
8. Y. Wang, Z. Feng, D. Laul, W. Zhu, M. Provencher, M. L. Trudeau, A. Guerfi and K. Zaghib, *J. Power Sources*, 2018, **374**, 211-216.
9. S. Qiu, X. Wu, M. Wang, M. Lucero, Y. Wang, J. Wang, Z. Yang, W. Xu, Q. Wang and M. Gu, *Nano Energy*, 2019, **64**, 103941.
10. J. Zhang, L. Chen, L. Niu, P. Jiang, G. Shao and Z. Liu, *ACS Appl. Mater. Interfaces*, 2019, **11**, 39757-39764.
11. P. Lei, K. Liu, X. Wan, D. Luo and X. Xiang, *Chem. Commun.*, 2019, **55**, 509-512.
12. F. Zhang, W. Li, X. Xiang and M. Sun, *Chem. Eur. J.*, 2017, **23**, 12944-12948.
13. Z. Li, D. Young, K. Xiang, W. C. Carter and Y. M. Chiang, *Adv. Energy Mater.*, 2013, **3**, 290-294.
14. P. Jiang, Z. Lei, L. Chen, X. Shao, X. Liang, J. Zhang, Y. Wang, J. Zhang, Z. Liu and J. Feng, *ACS Appl. Mater. Interfaces*, 2019, **11**, 28762-28768.
15. L. Suo, O. Borodin, Y. Wang, X. Rong, W. Sun, X. Fan, S. Xu, M. A. Schroeder, A. V. Cresce and F. Wang, *Adv. Energy Mater.*, 2017, **7**, 1701189.
16. Z. Hou, X. Li, J. Liang, Y. Zhu and Y. Qian, *J. Mater. Chem. A*, 2015, **3**, 1400-1404.
17. X. Wu, Y. Cao, X. Ai, J. Qian and H. Yang, *Electrochem. Commun.*, 2013, **31**, 145-148.
18. M. Shao, B. Wang, M. Liu, C. Wu, F.-S. Ke, X. Ai, H. Yang and J. Qian, *ACS Appl. Energy Mater.*, 2019, **2**, 5809-5815.